# Water sorption and heat storage in CaCl 2 impregnated Aluminium Fumarate MOFs

Quentin Touloumet, Lishil Silvester, Laurence Bois, Georgeta Postole, Aline Auroux

# Water sorption and heat storage in $CaCl_2$ impregnated Aluminium Fumarate MOFs

Quentin Touloumet [a], Lishil Silvester [b], Laurence Bois [b], Georgeta Postole [a,*], Aline Auroux [a,*]

[a] *Univ Lyon, Université Claude Bernard Lyon 1, CNRS, IRCELYON, F-69626 Villeurbanne, France*

[b] *Univ Lyon, Université Claude Bernard Lyon 1, CNRS, LMI, F-69622 Villeurbanne, France*

Corresponding authors: aline.auroux@ircelyon.univ-lyon1.fr
georgeta.postole@ircelyon.univ-lyon1.fr

Abstract

Composite materials based on aluminium fumarate (AF) and $CaCl_2$ have been developed for the storage of energy from renewable and waste sources. Composite Salt-Porous Matrix (CSPM) was synthesised by impregnating aluminium fumarate MOF host matrix with various relative $CaCl_2$ salt contents (25-60 wt.%). The resulting CSPMs were fully characterized by X-ray diffraction, $N_2$ and $H_2O$ sorption isotherms at −196 and 25 °C, respectively, scanning electron microscopy and thermal analysis. The high surface area of the AF matrix (959 $m^2\ g^{-1}$) drastically decreases upon the addition of salt, to about 50 $m^2\ g^{-1}$. The heat storage performance of the composites was found to depend on the added amount of salt to the MOF matrix, with higher amounts of salt leading to better performance. The maximum water sorption capacity of 0.68 $kg_{H_2O}\ kg^{-1}$, coupled with a high heat of water sorption (1840 kJ $kg^{-1}$), makes these composites interesting when used at a rehydration level not exceeding $CaCl_2.4H_2O$ to avoid any deliquescence and washing out of the salt. A kinetic study of the hydration demonstrated that salt deposition increases the water sorption rate in comparison with the host matrix. Moreover, the impact of salt deposition on the activation energy of dehydration of the host matrix was also determined by applying integral isoconversional methods.

*Keywords:* Thermochemical heat storage, MOF, Aluminium fumarate, Calcium chloride, Water sorption, Calorimetry

## 1. Introduction

One of the key issues around climate change and its environmental and socio-economic impacts is the strong dependence of our society on fossil fuels (~80% of the primary energy sources in the world) [1]. The transportation sector is the main consumer of primary energy (33%), followed by industry (31%) and residential (20%) uses [2]. In the European Union, heating and cooling account for half of the total final energy demand [3]. Generally, the recovery and storage of heat from waste sources (e.g. heat from engine exhaust gases, industrial waste heat,…) and the use of sustainable renewable energy would contribute to decrease dependency on fossil fuels and help lower the carbon footprint. However, the use of such energy sources for heating and cooling is very low, despite of their high potential in terms of energy storage. Renewable energies (wind, solar…) although clean, abundant and decentralised, require storage systems due to their intermittent character, often offering their highest potential during low demand periods [4]. Because thermal energy dominates the final energy use, thermal energy storage is an attractive technology in order to transfer surplus energy from waste heat and/or renewable energy sources and release it at times of high demand. It presents the advantage of a wide range of storage possibilities (sensible [5], latent [6], and thermochemical [7] heat storage) with storage periods ranging from minutes to months [8].

Thermochemical heat storage (TCHS) systems are one of the most promising technology among the available heat storage mechanisms due to their ability to achieve a high storage density (even with low temperature variations) over long time periods [9-12]. The basic configuration and operation of TCHS are well described in the literature [13-15]. Briefly, TCHS implies the use of physical or chemical bonds to store energy and operates via reversible sorption (e.g. solid/gas) reactions. TCHS systems mostly use a salt hydrate as thermal energy storage medium and water as reactive gas. During the charging process, heat (solar or low grade waste heat) is supplied to a TCHS material that decomposes into its two components, *sorbent* and *sorptive*, via an endothermic reaction. During the discharging process, the *sorbent* and *sorptive* react via an exothermic reaction that releases the stored heat [4,16]. Salt hydrates are environmentally safe, have a low cost, and present high affinity for water providing a suitable heat storage capacity for TCHS applications. However, most of the salt melts congruently with the formation of less hydrated forms, leading to an irreversible process and a continuous decrease in storage efficiency [17]. This phenomenon is also associated with agglomeration of the salt and washing out of active materials during TCHS use [11,18].

To overcome this main issue, water stable microporous and mesoporous adsorbents such as silica, alumina, zeolite, expanded vermiculite, aerogel, silico-aluminophosphates have been widely studied as heat storage materials [7,19-21]. The hydrophilic character, high affinity for water vapor, and large water sorption capacity at low relative humidity make silica gels promising candidates [22,23]. Microporous zeolites 3A, 4A, faujasites X and Y and alkali/alkaline earth metal modified zeolites have all been reported to be promising materials due to high water capacities at low relative pressure (0.05 - 0.3) and a high thermal stability. Jänchen et al. [19] reported sorption capacities of 0.24 $kg_{H_2O}$ $kg^{-1}$ and 0.19 $kg_{H_2O}$ $kg^{-1}$ for Li-X

and Na-X, respectively, while zeolite 4A showed a water sorption capacity of 0.22 $kg_{H_2O}$ $kg^{-1}$ [24]. Furthermore, the water sorption and heat storage capacities of different classes of materials such as aluminophosphates (AlPOs) and silicoaluminophosphates (SAPOs) have also been investigated [20,25]. The good thermal stability over successive hydration/dehydration cycles of these materials represents the main advantage for their use as component in thermochemical heat storage systems [26]. However, porous adsorbents have relatively low water sorption capacities compared to hygroscopic salts, and poor energy storage properties [27-30].

Aiming to overcome the issues of both classes of materials for TCHS applications, composite materials have been developed comprising hygroscopic salt hydrate inside a porous adsorbent solid as host matrix (CSPM, Composite Salt-Porous Matrix) [31-34]. Such composites take advantage of a combination of different water sorption mechanisms: heterogeneous adsorption on the host matrix surface, chemical reaction between salt and water to form hydrates, and liquid absorption by salt aqueous solution inside the pores [32]. Hence, the addition of salt hydrates to a porous matrix increases both the quantity of sorbed water and the heat storage capacity of the CSPM material.

Typical hygroscopic salt hydrates that can be incorporated into the porous host matrix include LiCl, $SrBr_2$, $MgSO_4$, $MgCl_2$ and $CaCl_2$ [8]. $CaCl_2$ is able to absorb water molecules at room temperature, to release water when heated providing high energy storage performances [33-35]. Composite materials containing calcium chloride exhibit the highest storage capacities [36] and seem to be the most promising candidates among the different salt hydrates used for thermal storage applications [37,38]. In particular, several composite materials containing $CaCl_2.6H_2O$ salt have been investigated in heat storage applications. Jabbari-Hichri et al. [37] reported that silica gel impregnated by 13.8 wt.% of $CaCl_2$ has a dehydration enthalpy and a water sorption capacity of 746 kJ $kg^{-1}$ and 0.27 $kg_{H_2O}$ $kg^{-1}$, respectively. Also, 14.0 wt.% $CaCl_2$ impregnated mesoporous alumina composite has shown a dehydration enthalpy of 576 kJ $kg^{-1}$ and a water sorption capacity of 0.17 $kg_{H_2O}$ $kg^{-1}$. Ristic et al. [39] demonstrated that the impregnation of mesoporous iron silicate (FeKIL2) with $CaCl_2$ triples the water sorption capacity of the support at high relative water vapour pressure.

Recently, Metal-Organic Frameworks (MOFs), a new type of porous materials, have gained much attention [40,41]. These materials are crystalline inorganic-organic hybrid materials, composed of inorganic metal ions or metal clusters linked by organic ligands through coordinate bonds [42]. MOFs have been successfully employed in applications such as catalysis [43], gas storage [44, 45] and drug delivery [46] thanks to their high surface area [47], low density, milder synthesis conditions and tunable properties [48-50]. These specific properties can make MOFs promising host porous materials for water and heat storage because they can surpass classical porous matrices like zeolites and silica gels in water sorption capacity. A metal-organic framework was firstly proposed as a solid adsorbent in heat transformation cycles for refrigeration, heat pumping, and heat storage by Henninger et al. [51] in 2009. Since then, a series of MILs (Materials from Institut Lavoisier) have been investigated for water sorption applications [53-55]. Kaskel and coworkers [52] reported that mesoporous MIL-100 (Fe) and MIL-101 have a water sorption capacity of 0.65 and 1.02 $kg_{H_2O}$ $kg^{-1}$, respectively. Permyakova et al. [53] studied the water sorption and heat storage capacities of $CaCl_2$ impregnated MIL and UIO (Material form University of Oslo)

composites. They reported that the increase of salt content in MOFs significantly enhances the water adsorption and the energy storage capacities. Shi et al. [54] determined that hydrophilic MOF based composite (MIL-101(Cr)-$SO_3H$/$CaCl_2$) has higher water sorption capacity (0.6 $kg_{H_2O}$ $kg^{-1}$) and a higher heat storage capacity (1274 kJ $kg^{-1}$) compared to pure host matrix MIL-101(Cr)-$SO_3H$ (0.43 $kg_{H_2O}$ $kg^{-1}$ and 694 kJ $kg^{-1}$). Among various MOFs used in thermochemical heat storage, aluminium fumarate has gained attention due to its high hydrophilicity, excellent multicycle stability, the lack of harmful components (heavy metal or critical organic compounds) and environmentally friendly synthesis route [55]. The possibility of a large scale production due to an easy and reproductible synthesis process also offers an important advantage [56]. The structure is made of infinite Al-OH-Al chains connected by fumarate linker. Aluminium fumarate 3D structure consists of [Al(OH)($O_2C$-CH=CH-$CO_2$)] with rhombohedral channels [57]. Also, the microporous structure of aluminium fumarate facilitates continuous pore filling with water while avoiding irreversible capillary condensation [58-60].

The present paper deals with a first attempt to use aluminium fumarate as a host matrix for calcium chloride, for thermochemical heat storage system applications. The impact of salt deposition on the structural and morphological properties and the hydrophilicity/hydrophobicity balance are investigated. The water and heat storage performances of the materials have been analysed using thermogravimetry (TG) coupled with differential scanning calorimetry (DSC) during two successive hydration/dehydration cycles. Furthermore, kinetic models have been applied to the experimental hydration and dehydration in order to get a better understanding of the impact of salt loading on sorption and desorption behaviours.

## 2. Experimental Section

### *2.1. Materials synthesis*

Aluminium chloride ($AlCl_3.6H_2O$), fumaric acid and $CaCl_2.2H_2O$ (in fact, $CaCl_2.xH_2O$ with $x \geq 2$ because of the hygroscopic character of $CaCl_2.2H_2O$) used in this study were purchased from Alfa Aesar. Aluminium fumarate (AF) was prepared according to the procedure already reported by El-Sayed et al. [59] and Teo et al. [57]. 0.36 g of $AlCl_3.6H_2O$ and 0.33 g of fumaric acid were dissolved in DMF (5 mL) before the mixture was heated in an autoclave at 150 °C for 15 h. The product was then separated by centrifugation, washed three times in ethanol, dried overnight at 80 °C and heated at 200 °C for 2 h.

The incorporation of $CaCl_2$ into the prepared AF matrix was performed by successive impregnations. In detail, 0.25, 0.50, and 1.5 mL of 1 M $CaCl_2.2H_2O$ solution in ethanol were added (in 0.25 mL steps) at room temperature to 0.1 g aluminium fumarate powder. Evaporation of ethanol was carried out between each step. Then, the $CaCl_2$-loaded AF composites were dried at 100 °C overnight. The loaded masses of $CaCl_2$ into AF, as determined by chemical analysis, were 25, 37 and 58 wt.%. Hereafter, the three synthesized composites are named as AF-$Ca_1$, AF-$Ca_2$ and AF-$Ca_3$ for 25, 37 and 58 wt.% $CaCl_2$ content, respectively. To remove $CaCl_2$ from the AF, the composite was placed in water under stirring at room temperature, filtered from the solution and dried.

### 2.2. *Material characterisation*

The textural properties were determined from nitrogen adsorption/desorption isotherms obtained at -196 °C using a BelsorpMini (Bel Instruments, Japan) apparatus. Prior to experiments, the solids (about 0.08 g) were outgassed at 150 °C for 4 h in secondary vacuum. The specific surface areas ($S_{BET}$) were derived from the BET (Brunauer – Emmett – Teller) standard equation, using a method adapted for microporous compound (norm iso 9277). Total pore volume was estimated by converting the adsorption amount of liquid nitrogen into volume at a relative pressure of 0.98. The mesoporous volume was calculated from the adsorption branch of the isotherms using the Barrett-Joyner-Halenda (BJH) method between $P/P_0 = 0.42$ and 0.96.

In order to further characterize textural and sorption properties of the studied TCHS materials, water vapor sorption isotherms were measured using a Micromeritics 3 Flex apparatus. Between 0.110 and 0.150 g of solid, previously outgassed at 150 °C for 3 h, were used. For obtaining the isotherms, the samples were kept at a constant temperature of 25 °C with a relative humidity ranging from 0 to 98 %. The quantity of water uptake is expressed in kg of water vapor per kg of sample as a function of $P/P_0$ at 25 °C.

Powder X-ray diffraction (XRD) patterns were collected at room temperature, under air, using a PANalytical Xpert Pro diffractometer (The Netherlands, CuKα radiation at 1.54 Å). Diffractograms were collected at 2θ between 5 and 45° with steps of 0.016°. Phase identification was performed using the Basolite A520$^{TM}$ (commercial aluminum–fumarate MOF from BASF SE) diffraction pattern taken in the Cambridge university CSD database (identifier: DOYBEA). $CaCl_2.2H_2O$ and $CaCl_2.4H_2O$ patterns came from the HighScore data base (respectively JCPDS: 01-070-0385 and 01-072-1015).

Chemical analyses of calcium were performed using inductively coupled plasma optical emission spectroscopy (ICP–OES) with an ACTIVA spectrometer from Horiba JOBIN YVON. In order to dissolve them completely, the samples were treated with a mixture of inorganic acids ($H_2SO_4$ and $HNO_3$) at 300 °C. The expected errors on the ICP-OES device are estimated at ± 2 %. In order to evaluate the analysis reproducibility, the Ca content was determined twice for each composite, at different times, on the same sample batch. The found error is of ± 2.4 %.

The morphology of the solids was studied by scanning electron microscopy (SEM) on a Zeiss Merlin Compact microscope (Centre Technologique des Microstructures de l'Université de Lyon) operating at 2 kV and equipped with an energy-dispersive X-ray (EDX) spectrometer. EDX analyses were performed on about 10 different areas.

### 2.3. *Measurements of heat and water storage properties*

The water sorption and heat storage/release capacities of the materials were measured using a thermogravimetric analyser (TG) coupled to a differential scanning calorimeter (DSC) (Setaram SENSYS EVO TG-DSC) and a humidity generator (Setaram WETSYS). The thermogravimetric investigations (with a measuring range of ± 200 mg and a resolution of 0.02 µg) made it possible to determine the mass evolution versus time and temperature and the quantity of sorbed/desorbed water. The sorption equilibrium was considered to be achieved when a weight change of less than 0.5 % was measured over two consecutive 10 min intervals. In addition to the water uptake measurements using TG, the amount of heat

stored/released during the sorption processes was simultaneously determined from DSC (heat flow) curves. Since the aim was to test the composites under conditions as close as possible to those used in open heat storage systems, the experiments were carried out at atmospheric pressure under dry/humid air flow (air 5.0, purity 99.999 %, $H_2O$ < 5 ppm). The humidity ratio was measured with a precision of ± 0.3 % RH. The air gas flow rate in all measurements was set to 20 mL $min^{-1}$, bath and gas temperature in the humidity generator were set to 40 °C, the humidity ratio was 30% RH (corresponding to 0.96 kPa pure water vapour pressure at 25 °C), and around 8 mg of sample was used to carry out the dehydration/hydration experiments. The procedure used to evaluate the storage properties consisted of the following steps: (1) The fresh solid, placed in an open quartz cell, was dehydrated under dry air flow at 150 °C for 3 h (the temperature ramping from 25 to 150 °C being performed with 2 °C $min^{-1}$), in order to ensure that the different materials were in the same initial state at the beginning of the study. (2) After cooling to room temperature under the same gas atmosphere, the first hydration cycle was performed at 25 °C by switching from dry to humid air flow which was maintained for 16 h, in order to hydrate the materials under conditions similar to those in applications. (3) After 16 h, the gas flow was switched back from humid to dry air, still at 25 °C, and the first two steps repeated for the next dehydration/hydration cycle. The second hydration step was used to study the water uptake kinetics. The samples were used in the powder form with particles size fraction of 0.1–0.5 µm. Since the sample weight affects the water loading rate during rehydration (preliminary investigations, not shown), the same amount of samples has been used in order to compare the kinetics of different materials. Fitted curves and kinetic parameters were determined using the BoxLucas1 model in Origin. Studied materials fitted curves contained 10000 points in order to determine as precisely as possible the kinetic parameter. The study here focused on the relative comparison of the composites synthesized with regard to salt loading.

The dehydration temperature of 150 °C was selected in order to match the main sources of waste heat in industry, such as exhaust gases, steam condensate, cooling water, and drying, baking or curing ovens [61]. It also matches the functioning temperature of the solar-thermal tube collectors used to warm up the air necessary to dry up the storage material in a real system [29,37]. The hydration step using the aluminium fumarate-based composites resulted in a flat DSC peak, and the signal did not return to the initial base line even after 16 h. Due to the difficulties in accurately integrating such a signal, the enthalpy values obtained from dehydration cycles were used instead to determine the heat stored in the composites. The measured heat flow was corrected by subtracting the heat flow signal of a blank test (performed under the same conditions with empty crucibles prior to the measurements). The linear integration of the resulting heat flow signal was used to determine the heat in kJ $kg^{-1}$. The estimated error on the dehydration heat values was around ± 20 kJ $kg^{-1}$. The second dehydration step was also performed at different heating rates (2, 4, 6 and 8 °C $min^{-1}$) in order to determine the apparent dehydration activation energy by using Kissinger and Ozawa methods [62,63].

The evolution of the weight of the material during the second dehydration cycle was obtained by the Eq. (1). The amount of water sorbed at a given time by the dry composites was obtained with Eq. (2) while the water sorption capacity (SC) was determined with Eq. (3):

$$W = \frac{W_{(t)}}{W_{hyd}} \quad (1)$$

$$Y = \frac{(W_{(t)} - W_{dehyd})}{W_{dehyd}} \quad (2)$$

$$SC_{H_2O} = \frac{(W_{hyd} - W_{dehyd})}{W_{dehyd}} \quad (3)$$

where $W_{(t)}$ represents the weight of the material measured at time t, $W_{hyd}$ is the weight of the wet adsorbent as measured after the first hydration step, and $W_{dehyd}$ is adsorbent weight after the second dehydration step (dry state). The employed procedure allows to compare samples with the high salt amounts.

## 3. Results and discussion

### *3.1. Structural and textural properties*

The physico-chemical characteristics of all materials were determined by surface area and pore volume measurements, chemical analyses, X-ray diffraction (XRD) and scanning electron microscopy (SEM).

The $CaCl_2$ contents, specific surface areas ($S_{BET}$), mesoporous ($V_{meso}$) and total pore ($V_{porous}$) volumes are summarized in Table 1. Fig. 1 presents the $N_2$ adsorption/desorption isotherms of all the solids. Pure aluminium fumarate (AF) possesses a high specific surface area (959 $m^2$ $g^{-1}$), which is consistent with data already published [59,64]. It shows a type I isotherm that is characteristic of microporous materials according to the I.U.P.A.C. classification [65]. Indeed, the adsorption isotherm is characterized by a rapid increase of the amount of gas adsorbed at low equilibrium pressures ($P/P_0$ = 0.02) which indicates the existence of a large number of micropores with a diameter lower than 2 nm. The following slow and continuous increase of the amount of $N_2$ adsorbed and the light hysteresis loop observed at $P/P_0 > 0.5$ disclose the emergence of a small number of narrow mesopores. The condensation of $N_2$ into the pores takes place at $P/P_0 > 0.9$. From Table 1, the AF sample presents high percentage (~87%) of microporous volume with respect to the total porous volume.

It can be noticed that introducing $CaCl_2$ to AF MOF induced a drastic decrease of the specific surface area and pore volume for all composites, as illustrated in Table 1. The significant reduction in the available pore volume could be caused by the salt accommodation inside the pores of the host material. Considering the pore volume of the matrix, the salt content in the composite (as determined by chemical analysis) and assuming that the salt occupies the difference of pore volume between the matrix and composite, the composite pore volume can be extracted from the Eq. (4) [66]:

$$CaCl_{2\ content}(CA) = \frac{V_{pmatrix} - V_{pcomposite}}{V_{pmatrix} + \frac{1}{\rho_{salt}}} \quad (4)$$

where $V_p$ is the pore volume and $\rho_{salt}$ the density of anhydrous $CaCl_2$ (2.15 g $cm^{-3}$ [27]). According to this equation, empty pore volumes should be 0.29 and 0.17 $cm^3$ $g^{-1}$ for the AF-$Ca_1$ and AF-$Ca_2$ composites, respectively and should correspond to a water sorption capacity of 0.29 $kg_{H_2O}$ $kg^{-1}$ and 0.17 $kg_{H_2O}$ $kg^{-1}$, respectively. The measured empty pore volumes (0.07 and 0.08 $cm^3$ $g^{-1}$ for the AF-$Ca_1$ and AF-$Ca_2$, respectively, Table 1) in the composites are not consistent with the theoretical values. It is likely that part of the host material pores is occupied by the introduced salt and thus, the salt is blocking the access and dramatically decreasing the $N_2$ adsorption capacity (Fig. 1). This indicates that the deposited salt in AF-$Ca_1$ and AF-$Ca_2$ is not located only inside the AF porosity but also in the inter-particle space of AF particles. Surprisingly, higher specific surface area and pore volume were found for AF-$Ca_3$ in comparison with those of the two other CSPMs, in spite of the highest salt loading. This can be explained by the bad dispersion of $CaCl_2$, located on the outer surface of the matrix instead to be located in the AF porosity leaving some host material pores access free. Besides, in Fig. 1 the tailing of hysteresis loop in the $N_2$ adsorption/desorption curves of this composite may arise from the formation of porous plugs in the pores of AF caused by impregnated salts.

**Table 1:** Physico-chemical characteristics of host matrix and corresponding composites.

| Sample | $CaCl_2$ content (wt.%)[a] | $S_{BET}$ ($m^2$ $g^{-1}$) | $V_{porous}$ ($cm^3$ $g^{-1}$)[b] | $V_{meso}$ ($cm^3$ $g^{-1}$)[c] |
|---|---|---|---|---|
| AF | 0 | 959 | 0.54 | 0.07 |
| AF-$Ca_1$ | 25 | 57 | 0.07 | 0.03 |
| AF-$Ca_2$ | 37 | 44 | 0.08 | 0.06 |
| AF-$Ca_3$ | 58 | 107 | 0.18 | 0.08 |

[a] Values determined using cation (wt.%) content determined by ICP-OES. [b] Determined from BET equation. [c] Determined from BJH method applied to the adsorption branch of the isotherm.

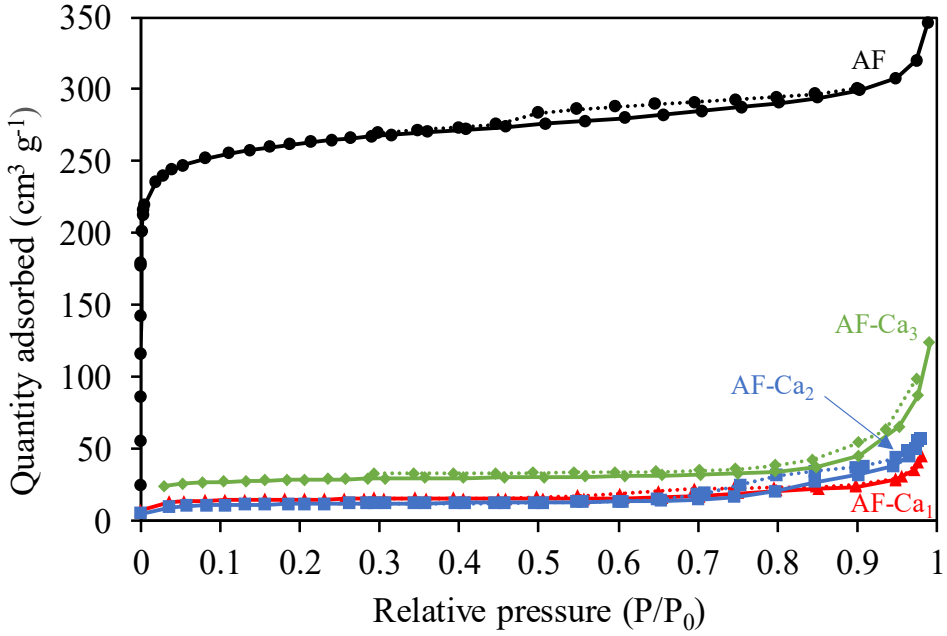


**Fig. 1.** $N_2$ adsorption/desorption isotherms of studied materials.

Fig. 2 shows the diffractograms of all synthesized solids along with the commercial Basolite A520™ (the aluminium fumarate marketed by BASF SE) as reference. The X-ray diffraction pattern of pure aluminium fumarate (AF) displays an intense peak at $2\theta$ = 10.3° and four well-resolved ones at 14.7°, 20.8°, 31.5° and 42.5°, which correspond to the intensity of Al ions in the aluminium fumarate structure. This result, in good agreement with the XRD pattern of Basolite A520™ and consistent with the diffraction patterns reported in the literature for aluminium fumarate MOF [55,57,64], shows that the AF matrix was properly synthesized with a stable structure.

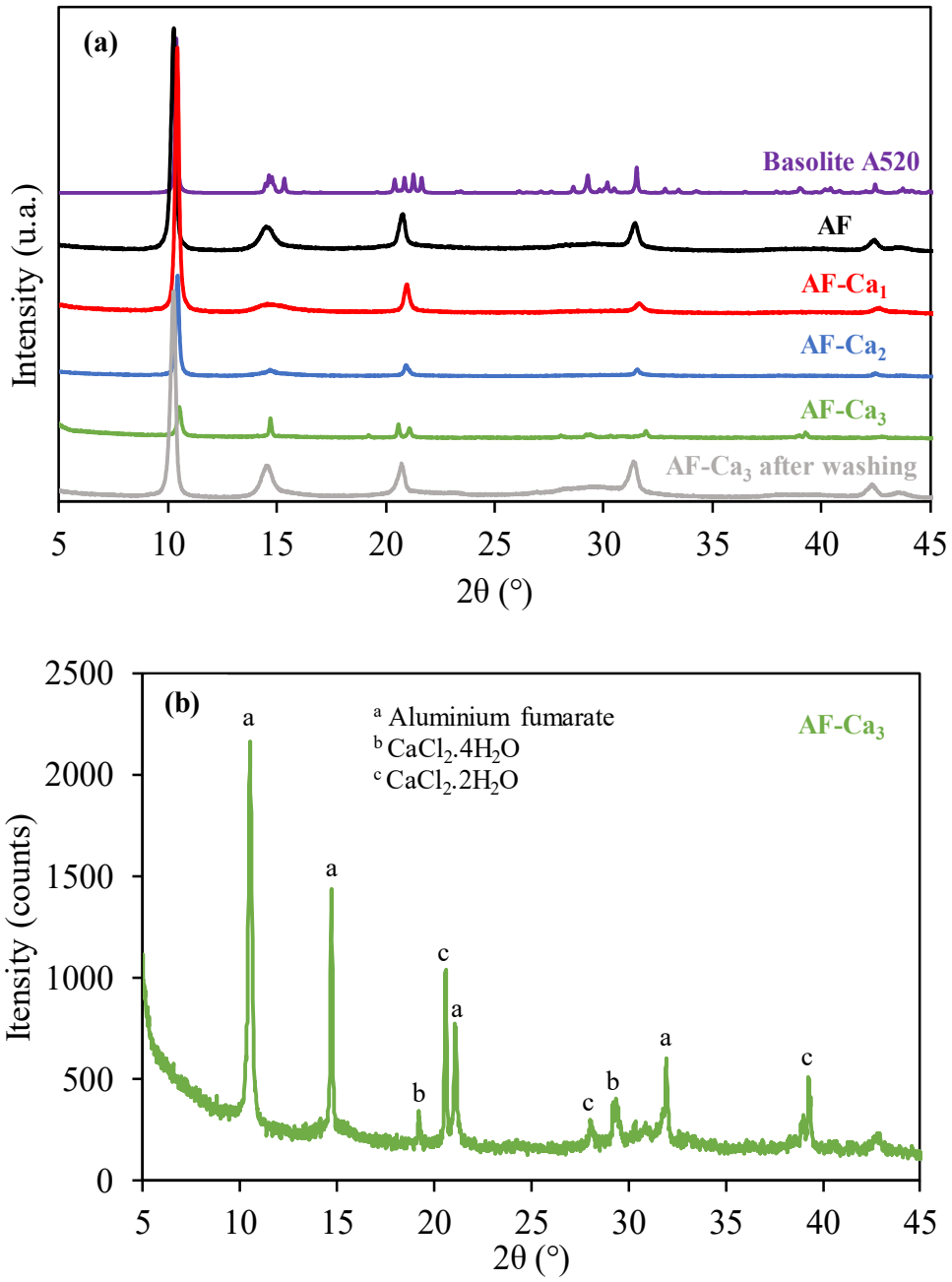


**Fig. 2.** XRD pattern of Basolite A520™ from Cambridge university database and experimental XRD patterns of AF, AF-$Ca_1$, AF-$Ca_2$ and AF-$Ca_3$ (a) and identification of XRD peaks of AF-$Ca_3$ (b).

Impregnating the AF matrix with $CaCl_2$ salt induced a small shift of the diffraction Bragg peaks of the host material to higher angles and the intensity of these peaks was decreased with increasing the $CaCl_2$ loading content. For the composite with the highest $CaCl_2$ content (58 wt.% in AF-$Ca_3$), the XRD characteristic peaks of the aluminium fumarate almost vanished. This could be explained by (i) an electronic density modification, (ii) a partial destruction of the AF structure or (iii) simply by an excess of salt [53]. Retention of the aluminium fumarate

MOF porous structure after introducing $CaCl_2$ was evidenced by XRD patterns obtained after dissolving and removing calcium chloride (see for example AF-$Ca_3$ washed in Fig. 2). X-ray diffraction pattern was completely restored as the initial AF matrix. The guest salt located inside the host material porosity may also induce changes in the AF lattice parameters and a shift of the reflexion peaks towards higher $2\theta$ (the rapid water sorption during the acquisition which induces a modification of the sample's thickness could also contribute to the observed shift). No diffraction peaks corresponding to $CaCl_2$ were observed in the XRD patterns of AF-$Ca_1$ and AF-$Ca_2$ composites containing 25 and 37 wt.% of salt, respectively. This could be explained by (i) the presence of highly dispersed $CaCl_2$ with nanosized dimensions that are not detectable by XRD technique and are located on the surface and within the matrix porosity or (ii) the formation, due to the high environmental relative humidity, of an amorphous salt phase as reported by Shi et al. [54] and Courbon et al. [27]. The presence of $CaCl_2.2H_2O$ and $CaCl_2.4H_2O$ diffraction peaks in AF-$Ca_3$ (58 wt.% $CaCl_2$) suggests that a portion of salt particles is located at the outer surface of the aluminium fumarate (Fig. 2b).

The samples morphology was studied by SEM imaging (Fig. 3). Examples of EDX analyses for the synthesized AF-$Ca_x$ composites are given in Fig. S1 together with the Ca/Al ratios. Aluminium fumarate shows agglomerated flattened spherical shape particles of 100-500 nm (Fig. 3a). The AF-Ca powders show different morphologies with the increase of the salt content. The AF-$Ca_1$ (Fig. 3b) presents similar morphology to that of AF and a homogeneous distribution of salt among the host matrix particles as determined by EDX analysis (Fig. S1a) giving a Ca/Al ratio (0.30 – 0.40 range) almost similar for all scanned areas of the composite. With increasing $CaCl_2$ loading, such as AF-$Ca_2$, a slightly more heterogeneous Ca/Al ratio (0.46 – 1.08 range) is determined which together with the formation of small agglomerates (Fig. 3c) accounts for a partial location of the salt particles within the interparticle pores of the host matrix. It is important to note that both AF-$Ca_1$ and AF-$Ca_2$ possess inter-cluster pores that can facilitate the diffusion of water vapor through the composite (Figs. 3b and c). The high amount of $CaCl_2$ deposited on AF in AF-$Ca_3$ led to the formation of large salt aggregates on the MOF surface (Fig. 3d) and its heterogeneous distribution among the host material particles (Ca/Al ratio between 1.18 and 3.90, as shown by EDX analyses (Fig. S1c). It is likely that the diffusion and location of the salt are affected and the host matrix pore volume is not completely accessible to the salt. It is noteworthy that the SEM micrograph of AF-$Ca_3$ after washing with water shows that the morphology of MOF crystallites is not altered by the salt loading (58 wt.%, Figs. 3a and e) thus confirming that the host material structure does not undergo major changes which is consistent with the XRD results.

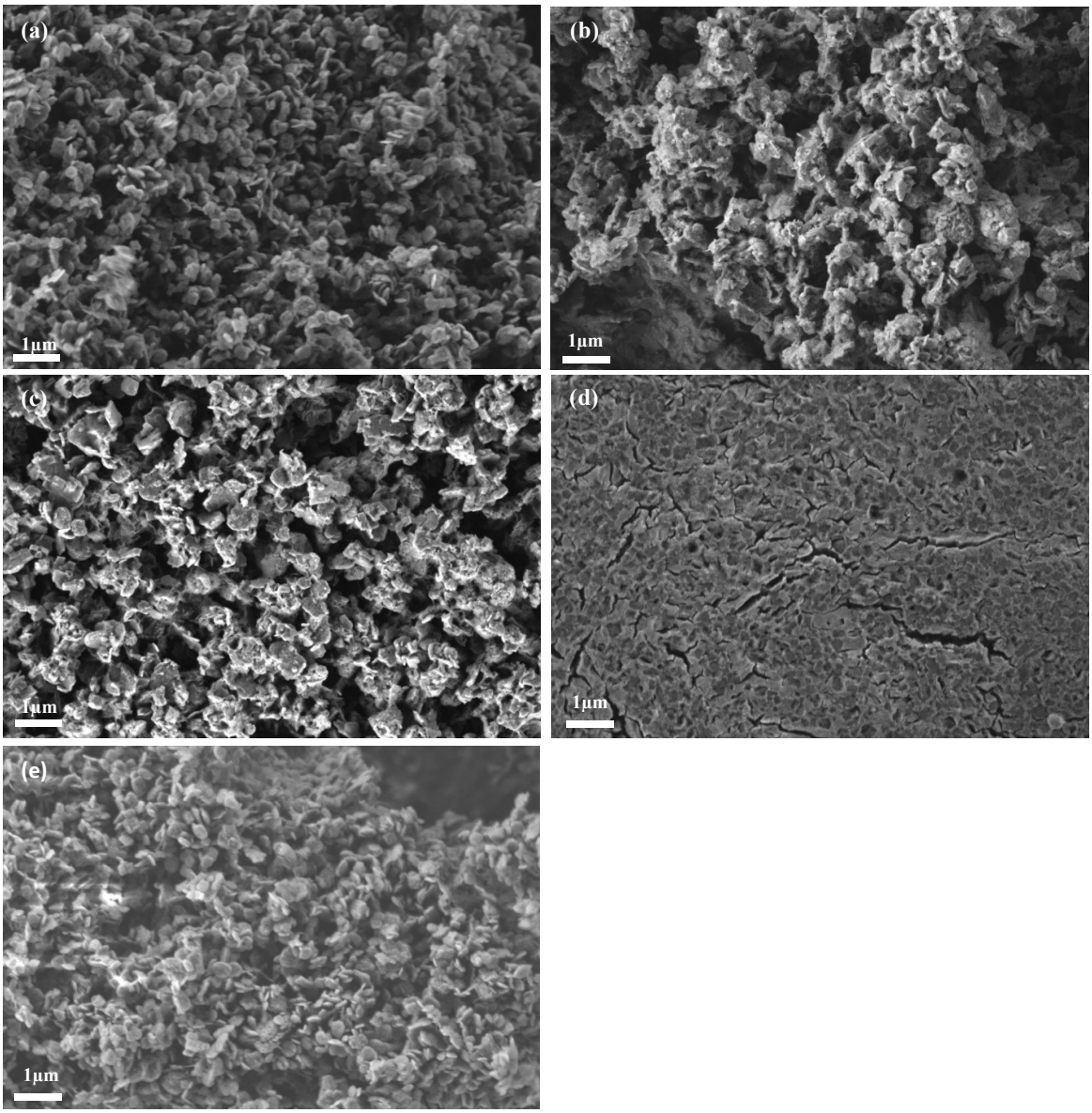


**Fig. 3.** SEM images of (a) AF, (b) AF-$Ca_1$, (c) AF-$Ca_2$, (d) AF-$Ca_3$ and (e) AF-$Ca_3$ after washing.

### *3.2. Water vapor isotherms*

The water sorption isotherms obtained for AF and the corresponding AF-$Ca_x$ composites are shown in Fig. 4. The AF isotherms exhibit three stages of adsorption/desorption that are characteristic of an "S"-shaped isotherm. At $P/P_0 < 0.2$, AF showed extremely low adsorption capacity; at $P/P_0$ between 0.2 to 0.3 an inflection point in the water uptake can be observed followed by a gentle rise between $P/P_0 = 0.3$ to 0.9. The desorption isotherm has almost the same trend as the adsorption behaviour with a narrow hysteresis being observed at low pressures. Some residual water seems to be trapped in the AF porosity. The good reversibility of the desorption phenomenon may arise from the relatively rigid structure of AF MOF due to

the fumarate conjugated system [57,67] and its predominant microporous character with pore diameters below 2 nm [60]. For thermochemical heat storage systems, the performance for water vapor adsorption at low RH is an important factor [68]. AF has short hydrophobic length ($0 \leq P/P_0 \leq 0.2$), in agreement with previous reports [57], and can be employed in thermochemical heat storage systems working at RH values starting from 30%.

Water sorption isotherms of bulk $CaCl_2$ display two step-like increases at $P/P_0$ of 0.11 and at $P/P_0$ of 0.2 indicating the formation of calcium chloride hydrates, which is consistent with calcium chloride hydration/dehydration isotherms already reported in the literature [27,69]. Courbon et al. [27] ascribed the first uptake step to the formation of $CaCl_2.2H_2O$ (R1) while the formation of calcium chloride tetrahydrate (R2) takes place in a second step. The third uptake step at $P/P_0 > 0.32$ is due to the formation of calcium chloride hexahydrate (R3) followed by progressive salt deliquescence and water absorption by the concentrated salt solution [70].

$$CaCl_{2(s)} + 2H_2O_{(g)} \longleftrightarrow CaCl_2.2H_2O_{(s)} \quad \text{(R1)}$$

$$CaCl_2.2H_2O_{(s)} + 2H_2O_{(g)} \longleftrightarrow CaCl_2.4H_2O_{(s)} \quad \text{(R2)}$$

$$CaCl_2.4H_2O_{(s)} + 2H_2O_{(g)} \longleftrightarrow CaCl_2.6H_2O_{(s)} \quad \text{(R3)}$$

The formation of $CaCl_2.1/3H_2O$ and $CaCl_2.H_2O$ hydration states [34,70] was not observed in our experimental conditions (Fig. S2). It can be explained by a too high-pressure first dose of water vapor at low relative pressure which leads directly in the formation of the dihydrated calcium chloride.

The three CSPMs exhibit an increased water uptake compared to AF which is beneficial for future TCHS applications. Indeed, besides an increase at low relative pressure, hygroscopic salt deposition on aluminium fumarate also enhances exponentially the water sorption capacity at high relative pressure. Generally, the isotherm curves of CSPMs exhibit a combination of the sorption features of both host matrix and deposited salt. The AF-$Ca_1$ isotherm curve displays a slight increase in the water uptake at $P/P_0 = 0.15$ associated to the water sorption on surface hydrophilic sites related to the presence of $CaCl_2$. The following gradual increase can be attributed to both AF pores filling and the formation of salt hydrates. By combining such hygroscopic salt and AF as host matrix, a water uptake of 1.18 $kg_{H_2O}$ $kg^{-1}$ is attained at high relative pressure ($P/P_0 = 0.9$) in AF-$Ca_1$, whereas AF has a water uptake of 0.43 $kg_{H_2O}$ $kg^{-1}$ at the same pressure. This significant improvement in water uptake capacity at high relative pressure is a characteristic of CSPMs [71] and can take place without significant salt deposition on the external surface of the matrix [72]. The water sorption isotherm of AF-$Ca_2$ shows a similar behaviour to AF-$Ca_1$ at low relative pressures ($P/P_0 < 0.5$). However, at higher relative pressures ($P/P_0 > 0.5$) the sorbed water uptake capacity is higher for AF-$Ca_2$ and increases exponentially to reach 1.97 $kg_{H_2O}$ $kg^{-1}$ at $P/P_0 = 0.9$.

Both composites present a minor irreversibility (i.e. the sorption and desorption branches do not match perfectly) which may arise from the weak flexibility of the AF framework. AF-$Ca_3$ with maximum salt loading displayed the highest water uptake capacity compared to the other composites in the whole range of relative pressure. The large water uptake of composites obtained at $P/P_0 = 0.9$ may corresponds to the water sorbed by the salt

located outside composites pores. However, at low relative pressures up to of 0.32 (the thermochemical properties are studied here at 30 % RH), this composite match or surpass $CaCl_2$ in water uptake. Contrary to its counterparts with lower amount of salt, AF-$Ca_3$ presents a significant hysteresis loop caused by the strong affinity of calcium chloride for water and the recrystallization steps. These results demonstrate that the salt content in the composites and the location of the salt have significant influence on the water sorption behaviour and performance.

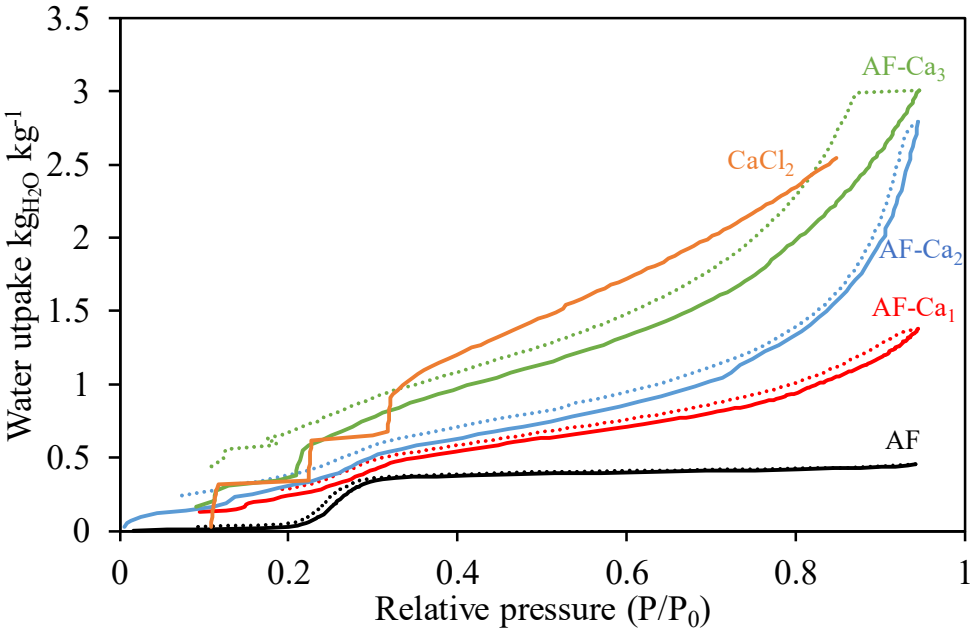


**Fig. 4.** Water sorption/desorption isotherms at 25 °C of AF, $CaCl_2$ and synthesized composites.

The hydrophilicity/hydrophobicity balance of microporous solids (e.g. MOFs exhibiting different pore size, topology and surface functions) can be determined, as reported by Canivet et al. [73], by taking into account three quantitative indicators. Firstly, the Henry constant ($K_H$) represents the affinity of water towards the solid surfaces and is determined by linear regression of the sorption isotherms at low relative pressure ($P/P_0 < 0.1$, using at least 3 data points, Figs S3-S5). The second indicator is the relative pressure $\alpha = P/P_0$ at which half of the total water uptake capacity is attained. This indicator is inversely proportional to the material hydrophilicity and is rather linked to the pore size distribution. Finally, the third indicator is the water uptake capacity ($kg_{H_2O}$ $kg^{-1}$) at $P/P_0 = 0.9$. Taking into account the combination of both physical and chemical sorption of water in the composites, only the former ($K_H$) and the last indicators (water uptake capacity at $P/P_0 = 0.9$) are given in Table 2. Furthermore, for relevant results, only the composite materials with a similar morphology to AF (i.e., AF-$Ca_1$ and AF-$Ca_2$) are compared. A too high water uptake by $CaCl_2$, at low relative pressures, in AF-$Ca_3$ does not allow the determination of Henry constant and thus a direct comparison with the other solids. The determined Henry constant of AF is of the same

order as Al-MIL-53 (1.17 x $10^{-6}$ mol $g^{-1}$ $Pa^{-1}$ [73]]) presenting similar crystal structure with octahedral $AlO_4(OH)_2$ units connected through 1,4-benzenedicarboxylate ligands. Besides, the value of the alpha indicator of AF ($\alpha = 0.26$) also corresponds to those previously reported for other MOF hydrophilic materials (e.g. $\alpha = 0.25$ for Ti-MIL-125) [73]. After salt impregnation, the composites are characterized by an enhanced surface affinity for water, as indicated by the evolution of the Henry constants ($K_H$ = 2.0 x $10^{-6}$ mol $g^{-1}$ $Pa^{-1}$ for AF *vs* $K_H$ = 1.0 x $10^{-5}$ and 2.0 x $10^{-4}$ mol $g^{-1}$ $Pa^{-1}$ for respectively AF-$Ca_1$ and AF-$Ca_2$) and the water uptake capacity at $P/P_0$ = 0.9 (Table 2).

**Table 2:** Hydrophilicity/hydrophobicity indicators of AF, AF-$Ca_1$ and AF-$Ca_2$.

| Material | $K_H$ (mol $g^{-1}$ $Pa^{-1}$)[a] | Log ($K_H$) | Water uptake ($kg_{H_2O}$ $kg^{-1}$)[b] |
|---|---|---|---|
| AF | 2.0 x $10^{-6}$ | -5,7 | 0.43 |
| AF-$Ca_1$ | 1.0 x$10^{-5}$ | -5,0 | 1.18 |
| AF-$Ca_2$ | 2.0 x$10^{-4}$ | -3,7 | 1.97 |

[a] 5% experimental error. [b] Water uptake at $P/P_0$ = 0.9.

### *3.3 TG-DSC results*

#### *3.3.1 Dehydration TG-DSC study*

Changes in the mass of the solids during the dehydration/hydration cycles have been studied using thermogravimetric analysis. Fig. 5 shows the mass variations of the solids during the second dehydration. All materials exhibited weight loss during dehydration due to the removal of water sorbed during the first hydration cycle. The weight loss increased with increasing salt loading and followed the order: AF < AF-$Ca_1$ < AF-$Ca_2$ < AF-$Ca_3$. This behaviour is explained by the high capacity of the hygroscopic salt to react with water [35]. The water sorption performance of CSPMs is thus directly related to the amount of hygroscopic salt in the composite.

With rehydration procedure used in this study, commercial $CaCl_2.2H_2O$ allows to regain 2.7 water molecules, which is consistent with data already published and is justified by a partial rehydration to $CaCl_2.4H_2O$ [39]. $CaCl_2.2.7H_2O$ has a higher water sorption capacity than AF-$Ca_1$ (25 wt.% salt) but lower than AF-$Ca_2$ and AF-$Ca_3$ containing, respectively, 37 and 58 wt.% of $CaCl_2$. All the solids exhibited complete weight loss within at most 20 min of dehydration at 150 °C, which is suitable for thermochemical heat storage applications [8].

The dehydration reactions of aluminium fumarate and corresponding composite materials are complex processes, involving consecutive transformations between different phases of each hydrated material. The water mass loss of $H_2O$ was measured for each well-defined single dehydration step, leading to the determination of the overall amount of water sorbed by the material in experimental conditions (see Table 3, column 3).

From DSC results, the dehydration process of $CaCl_2.2.7H_2O$ exhibits a thin endothermic peak with shoulders between 42 and 53 °C (Fig. 6) that are possibly due to $CaCl_2.4H_2O$ fusion

[74,75]. $CaCl_2.2.7H_2O$ displays two large overlapping signals between 100 to 150 °C, which overall is accompanied by the loss of 16.8 mol $kg^{-1}_{hyd}$ (mol of water per kg of initial hydrated material). During the dehydration process of aluminium fumarate, only one large endothermic peak is observed from 25 to 100 °C with a maximum at 83 °C and a shoulder at about 40 °C, corresponding to the loss of 10.6 mol $kg^{-1}_{hyd}$ (from Fig. 5). Taking into account the TG-DSC data of parent aluminium fumarate and $CaCl_2.2.7H_2O$ makes it possible to determine the dehydration process of the CSPMs. Namely, for all three CSPMs the dehydration process occurred in two steps, each accompanied by an endothermic DSC peak with or without shoulders. It can be assumed that the first endothermic peak corresponds roughly to dehydration of the support, followed by the second peak due to salt dehydration. Both AF-$Ca_1$ and AF-$Ca_2$ exhibited a large peak in the 25 – 110 °C temperature range corresponding to the support dehydration, followed by a second peak in the 110 – 150 °C temperature range attributed to the salt dehydration. For AF-$Ca_1$, out of a total of 15.4 mol $kg^{-1}_{hyd}$ desorbed, 12.8 mol of water correspond more or less to dehydration of the support, with the remaining 2.6 mol being assigned to salt dehydration. The amount of mol of water desorbed during each of the two dehydration stages of AF-$Ca_2$ is increased in comparison to AF-$Ca_1$: AF-$Ca_2$ exhibited an overall loss of 18.6 mol $kg^{-1}_{hyd,}$ of which support hydration amounted to 13.9 mol of water while the amount from salt hydration was around 4.7 (Fig. 5).

The amounts of water desorbed by the support in these composites (12.8 and 13.9 mol $kg^{-1}_{hyd}$ for AF-$Ca_1$ and AF-$Ca_2$ respectively) are higher than that of pure AF (10.6 mol $kg^{-1}_{hyd}$). This gap can be attributed to water sorption at the host material – salt interface. Due to the presence of the salt layer on the AF surface in AF-$Ca_3$ composite, the amount of desorbed water related to the support dehydration is much lower than for the two other composites. The composite with the highest salt loading (AF-$Ca_3$) desorbed 21.7 mol of water per kg of hydrated sample. The attributed support dehydration and the salt dehydration peaks of AF-$Ca_3$ correspond to the loss of 9.9 and 11.8 mol $kg^{-1}_{hyd}$, respectively. In summary, the TG-DSC results demonstrated the dual influence of both support and salt during dehydration of CSPMs, especially at the interface.

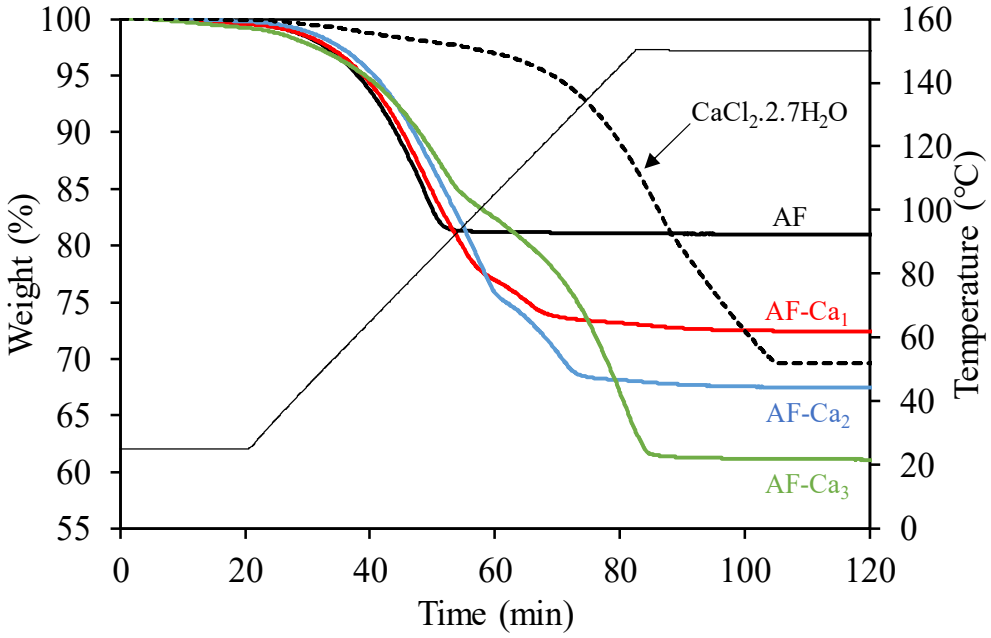


**Fig. 5.** Weight evolution during the second dehydration.

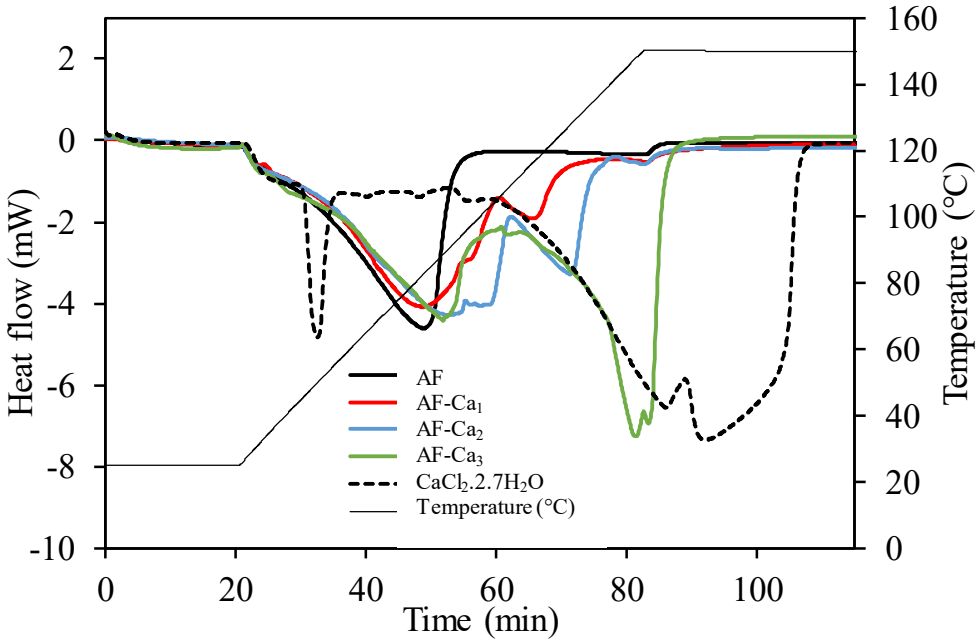


**Fig. 6.** DSC dehydration peaks of $CaCl_2.2.7H_2O$ and studied materials during the second dehydration.

### *3.3.2 Heat storage performance and water sorption properties*

The water sorption capacities of the studied materials and $CaCl_2.2.7H_2O$ were determined for 16 h hydration at 25 °C under 30 % RH and are expressed in terms of kg of sorbed water per kg of dehydrated materials as determined by Eq. (3). The energy storage capacity is

determined by integrating linearly the heat flow signal, after subtracting the heat flow signal of a blank test (performed under the same conditions with empty crucibles). Fig. 7 presents the heat storage (in kJ $kg^{-1}$ of dehydrated sample) and water sorption capacities (in kg of water $kg^{-1}$ of dehydrated sample) as a function of the $CaCl_2$ wt.% content. The composites exhibited higher heat storage and water sorption capacities compared to that of AF, which sorbed 0.27 ± 0.02 $kg_{H_2O}$ $kg^{-1}$ with an energy storage capacity of 638 ± 20 kJ $kg^{-1}$. The water sorption capacities of the AF-$Ca_x$ composites increased with $CaCl_2$ loading, and ranged from 0.37 ± 0.02 $kg_{H_2O}$ $kg^{-1}$ (25 wt.% $CaCl_2$) to 0.68 ± 0.02 $kg_{H_2O}$ $kg^{-1}$ (58 wt.% $CaCl_2$). Energy storage capacity increased gradually from 998 ± 20 kJ $kg^{-1}$ (AF-$Ca_1$) to 1840 ± 20 kJ $kg^{-1}$ (AF-$Ca_3$). As expected, an increase in the amount of $CaCl_2$ in the composite enhanced the water sorption capacity and consequently, the energy storage capacity in kJ $kg^{-1}$ [37,39,76]. Besides, the aluminium fumarate composites with higher amounts of salt (AF-$Ca_2$ and AF-$Ca_3$) show experimental dehydration heats higher than expected by simple addition of the two contributions of the salt and the support (as derived from the experiments performed on $CaCl_2.2H_2O$ and AF separately, Table 3). This is probably caused by stabilization of the salt by the aluminium fumarate matrix, thus minimizing salt agglomeration and leaching and shows the synergetic effect of the deposition of a hygroscopic salt on aluminium fumarate matrix. In terms of heat released per mol of water, an increase is also obtained after aluminium fumarate impregnation. Salt deposition improves the surface affinity of the solids for water, resulting in a more energetic process and thus higher values of the total heat released [77]. Expressed in kg $mol^{-1}{}_{H_2O}$, AF-$Ca_2$ shows the same heat storage capacity as AF-$Ca_3$, although it contains a lower amount of $CaCl_2$. The absence of a significant salt deposition on the external surface of aluminium fumarate matrix in AF-$Ca_2$, allows a better diffusion of adsorbed water molecules into the bulk composite. However, attention must be paid with the very hygroscopic salts, such as $CaCl_2$, that can be easily dissolved in water. Although, the heat of dissolution can increase the total heat value per mol of water, dissolution reduces the bed porosity of the material and thereby the vapor transportation through the bed, limiting the ability of the composite to rehydrate.

**Table 3:** Comparison of the storage performances of the solids.

| Solids | $CaCl_2$ content (wt.%) [a] | Water sorption capacity ($kg_{H_2O}$ $kg^{-1}$) [b] | $\Delta H_{dehydration}$ (kJ $kg^{-1}$) (experimental) [c] | $\Delta H_{dehydration}$ (kJ $kg^{-1}$) (calculated) [d] | $\Delta H_{dehydration}$ (kJ $mol^{-1}{}_{H_2O}$) [e] |
|---|---|---|---|---|---|
| $CaCl_2.2.7H_2O$ | - | 0.44 | 1540 | - | 63.4 |
| AF | 0 | 0.27 | 638 | - | 48.7 |
| AF-$Ca_1$ | 25 | 0.37 | 998 | 1023 | 47.4 |
| AF-$Ca_2$ | 37 | 0.49 | 1425 | 1208 | 52.6 |
| AF-$Ca_3$ | 58 | 0.68 | 1840 | 1531 | 52.2 |

[a] Determined by chemical analysis (± 2%). [b] Water sorption capacity determined with Eq. (3) on dehydrated sample at 150 °C (± 0.02). [c] Dehydration heat determined by 2nd dehydration heat flow integration (± 20 kJ $kg^{-1}$). [d] Dehydration heat calculated by addition of the heat contributions

(determined experimentally) of $CaCl_2$,2.7$H_2O$ and AF. [e] Dehydration heat expressed in kJ $mol^{-1}{}_{H_2O}$ (± 0.5 kJ $mol^{-1}$).

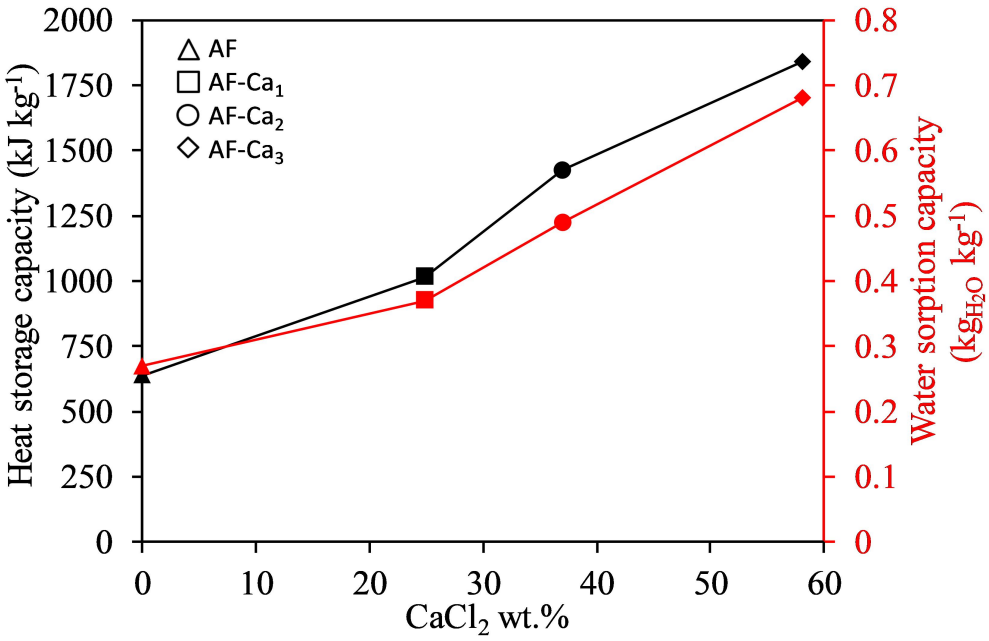


**Fig. 7.** Water sorption and heat storage capacities of the studied materials.

The water sorption and heat storage performances of our studied materials and some of previously reported $CaCl_2$-containing composites in the literature are summarized in Table 4. The energy storage performances of MOFs impregnated by 46 and 46.7 wt.% of calcium chloride did not exceed 1278 kJ $kg^{-1}$ [53,54]. However, Permyakova et al. [53] reported an energy storage capacity of 1746 ± 180 kJ $kg^{-1}$ for MIL-101(Cr) impregnated by 62 wt.% of $CaCl_2$. AF-$Ca_2$ (37 wt.% of $CaCl_2$) and AF-$Ca_3$ (58 wt.% of $CaCl_2$) reported in this study display higher or at least similar energy storage performances compared to the $CaCl_2$ - MOF based composites described so far in the literature. Moreover, AF-$Ca_2$ and AF-$Ca_3$ possess lower sorption capacities than the previously reported materials, once again demonstrating the high efficiency of aluminium fumarate-$CaCl_2$ composites for thermochemical heat storage.

**Table 4:** Comparison of storage performances between the studied materials and other composites in the literature.

| Host matrix | $CaCl_2$ content (wt.%) [a] | Hydration temperature (°C) | RH during hydration (%) | Dehydration temperature (°C) | Water sorption capacity ($kg_{H_2O}$ $kg^{-1}$)[b] | Heat storage capacity (kJ $kg^{-1}$)[c] | Ref. |
|---|---|---|---|---|---|---|---|
| AF | 0 | 25 | 30 | 150 | 0.27 | 638 | This work |
| AF-$Ca_1$ | 25 | 25 | 30 | 150 | 0.37 | 998 | This work |
| AF-$Ca_2$ | 37 | 25 | 30 | 150 | 0.49 | 1425 | This work |
| AF-$Ca_3$ | 58 | 25 | 30 | 150 | 0.68 | 1840 | This work |
| MIL-101(Cr) | 46.7 | 30 | 32 | 120 | 0.47 | 1118 | [54] |
| MIL-101(Cr)-$SO_3H$ | 43.1 | 30 | 32 | 120 | 0.60 | 1274 | [54] |
| MIL-100(Fe) | 46.0 | 30 | 30 | 80 | 0.57 | 1206 ± 72 | [53] |
| MIL-101(Cr) | 62.0 | 30 | 30 | 80 | 0.75 | 1746 ± 180 | [53] |
| Silica gel | 13.8 | 20 | 30 | 300 | 0.23 | 746 ± 15 | [33] |
| Alumina | 14.4 | 20 | 30 | 300 | 0.17 | 576 ± 15 | [33] |
| Zeolite Ca-X | 15.0 | 30 | 35 | 110 | 0.125 | 498 ± 20 | [71] |

[a] According to chemical analysis (± 2%). [b] Water sorption capacity determined with Eq. (3) (± 0.02)
[c] Heat storage determined with 2nd dehydration heat flow integration (± 20 kJ $kg^{-1}$).

Stability during five successive hydration/dehydration cycles was investigated under the same operating conditions employed in the above-mentioned two cycle experiments. Energy storage and water sorption capacities of the AF and AF-$Ca_3$ solids are shown in Figs 8a and b. As the first dehydration corresponds to the pre-treatment, only the storage performances of cycles 2 to 5 are presented here.

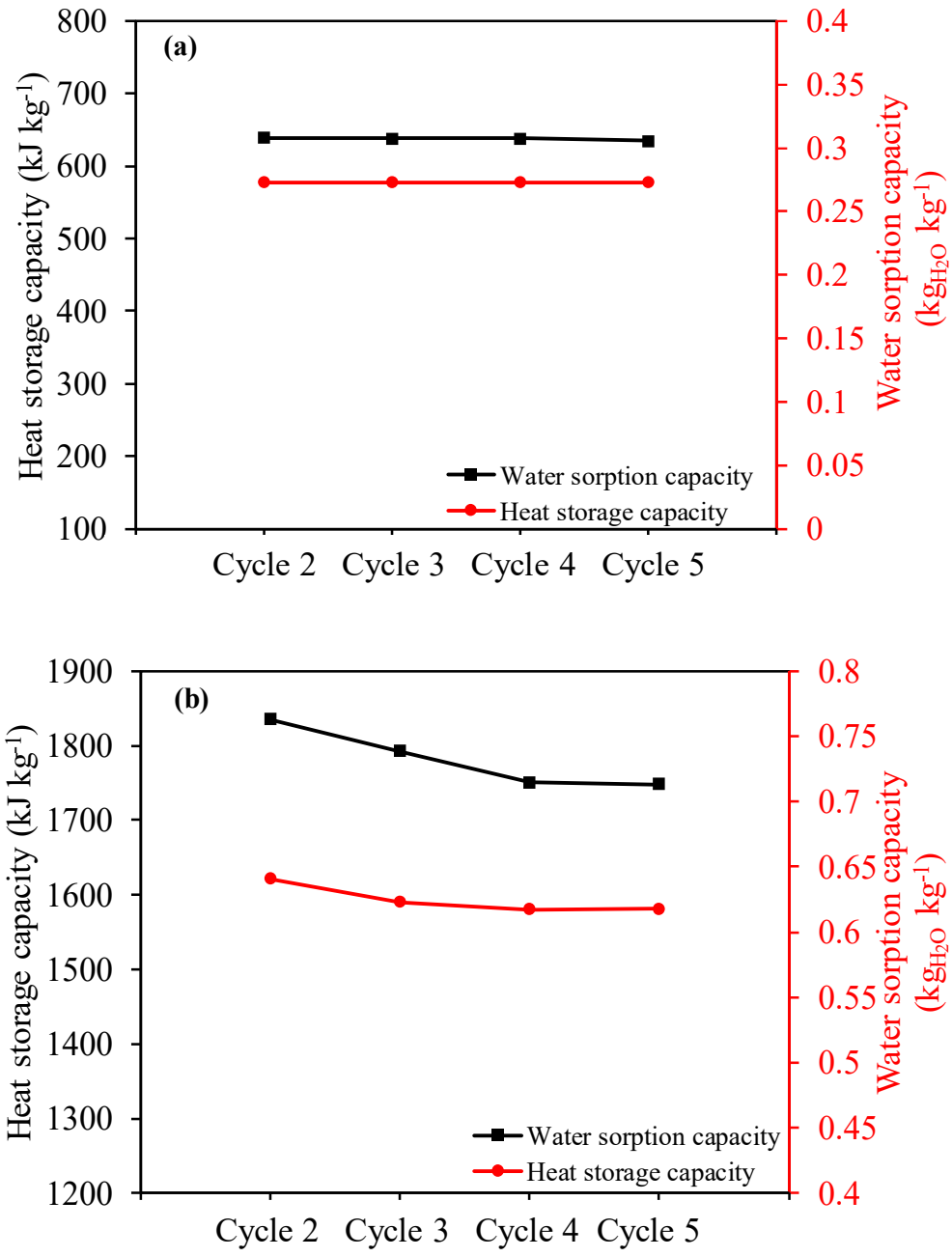


**Fig. 8.** AF (a) and AF-$Ca_3$ (b) stability over dehydration/hydration cycles.

AF, for the first time studied as porous matrix in TCHS applications, exhibits stable storage properties without any loss in water sorption and energy storage capacities during 5 adsorption/desorption cycles. Although the as synthesized AF-$Ca_3$ showed the presence of salt at the outer surface of AF, it exhibited only slight decrease (~5 to 6 %) in the water sorption and heat storage capacities during the first fourth cycles, which then remained rather steady at 1750 kJ $kg^{-1}$ with 0.62 $kg_{H_2O}$ $kg^{-1}$. Such stable energy storage performance for physical mixture of the salt and AF MOF with only part of $CaCl_2$ incorporated into the matrix porosity

suggests that the aluminium fumarate matrix contributes to the development of efficient CSPMs for thermochemical heat storage systems. It must be pointed out that the incomplete hydration of the salt (hydration level not exceeding $CaCl_2.xH_2O$ with $x \leq 4$) after 960 min in our experiments plays a key role in the observed stability. Stabilization of storage capacities of MOF composite materials after several dehydration/hydration cycles has been previously observed by Permyakova et al. [53] for completely incorporated salt in the MOF matrix.

### *3.4 Kinetic study*

#### *3.4.1 Water adsorption kinetics of the host matrix and composite materials*

Besides heat storage capacity and stability, water vapor sorption kinetics of CSPMs should be taken into consideration for elaborating and optimizing TCHS systems. Fig. 9 shows the water uptake as a function of time during the second hydration cycle of the studied materials obtained with Eq. (2). It is evident from the Fig. 9 that the saturation point of water uptake is not attained for all solids even after 16 h of hydration at 30 % relative humidity. Consequently, the maximum water uptake capacity and thus the energy storage capacity is not attained during hydration cycles with the experimental conditions employed.

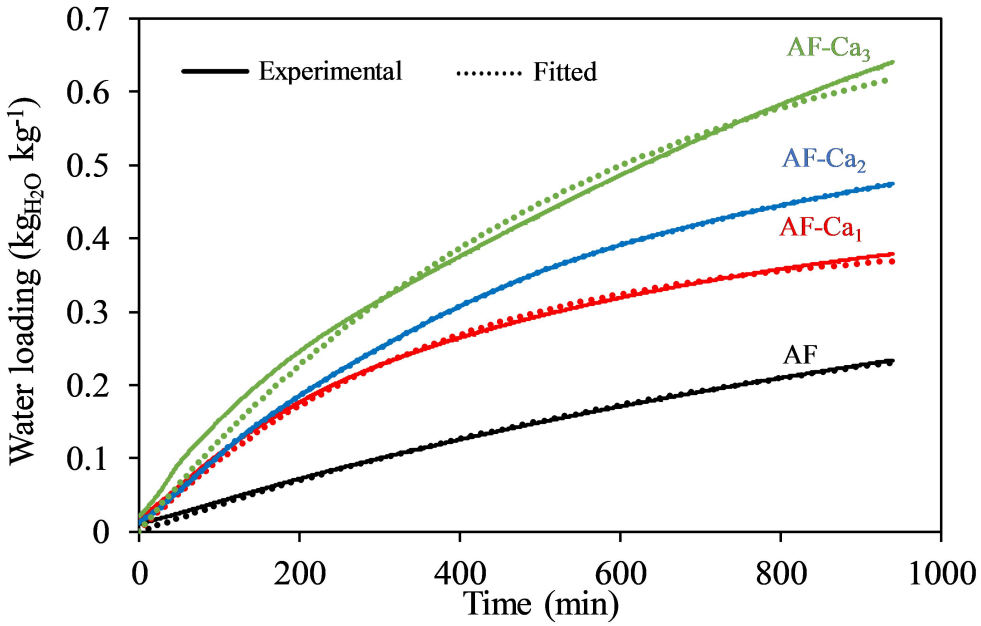


**Fig. 9.** Water adsorption kinetic curves of studied materials.

The water uptake over time of AF and corresponding composites were fitted well with a pseudo-first order model (Eq. (5), Fig. 9 and Table 5). Fitted curves and kinetic parameters were determined using the BoxLucas1 model in Origin.

$$W_{(t)} = W_e(1 - \exp(-kt)) \quad (5)$$

where $W_e$ represents the equilibrium water sorption quantity ($kg_{H_2O}$ $kg^{-1}$), $W_{(t)}$ represents the weight measured at time t ($kg_{H_2O}$ $kg^{-1}$), k stands for the rate coefficient ($min^{-1}$) and *t* for the time elapsed (min).

The presence of highly hygroscopic $CaCl_2$ enhances the surface affinity and hydrophilicity of composites, leading to a faster sorption rate. With increasing salt content, sorption rate coefficient of composites decreases progressively, mainly due to an increasing of salt particle water diffusion resistance. Although the salt is partly located outside of matrix porosity, the sorption rate of AF-$Ca_3$ is higher than that of pure AF. From Eq. (5), the calculated saturation water sorption quantity $W_{(e)}$ (for an infinite time at 30 % of relative humidity) can also be determined. $W_{(e)}$ is 0.37 $kg_{H_2O}$ $kg^{-1}$ for AF, and 0.40, 0.56 and 0.76 $kg_{H_2O}$ $kg^{-1}$ for the three CSPMs respectively (Table 5).

**Table 5:** Kinetic parameters form gravimetric water sorption over time.

| Sample | $W_e$ [a] ($kg_{H_2O}$ $kg^{-1}$) | k ($min^{-1}$) | $R^2$ [b] |
|---|---|---|---|
| AF | 0.37 ($6 \times 10^{-4}$) | $1.06 \times 10^{-3}$ ($2 \times 10^{-6}$) | 0.9982 |
| AF-$Ca_1$ | 0.40 ($2 \times 10^{-4}$) | $2.83 \times 10^{-3}$ ($4 \times 10^{-6}$) | 0.9964 |
| AF-$Ca_2$ | 0.56 ($1 \times 10^{-4}$) | $2.02 \times 10^{-3}$ ($9 \times 10^{-7}$) | 0.9998 |
| AF-$Ca_3$ | 0.76 ($1 \times 10^{-3}$) | $1.76 \times 10^{-3}$ ($5 \times 10^{-7}$) | 0.9915 |

[a] Obtained from fitting the gravimetric measurement (Eq. (2)) with Eq. (5) (cf: Fig. 9). [b] Standard deviations are given in parentheses.

### *3.4.2 Water desorption kinetic study*

The expression representing the kinetic control equation of non-isothermal reaction is given by Eq. (6) as reported by Vyazovkin et al. [78] from the concept of reaction order put forward by van't Hoff to various rate constant relations of Arrhenius.

$$\frac{d\alpha}{dT} = \left(\frac{A}{\beta}\right) \exp\left(\frac{-E}{RT}\right) f(\alpha) \quad (6)$$

where $\alpha$ represents the conversion percentage of reactant to product (namely the molar fraction reacted, as given in Eq. (7)), $T$ is the thermodynamic temperature, A is the pre-exponential factor, β is the heating rate, R is the molar gas constant, E is the apparent activation energy, $f(\alpha)$ is the mechanism function of reaction kinetics. In this equation, A, $\beta$, E and R are constants.

$$\alpha = \left(1 - \frac{W_{(t)}}{W_i}\right) \times \frac{M_h}{M_{H_2O}} \quad (7)$$

where $W_{(t)}$ represents the sample weight, $W_i$ is the initial weight of reactant, $M_h$ is the molecular weight of reactant (determined thanks to the dehydration equation) and $M_{H_2O}$ is the molecular weight of water. Two dehydration-hydration cycles have been performed using AF and AF-$Ca_3$ at different heating rates of 2, 4, 6 and 8 °C $min^{-1}$. Figs. 10a and b present the relation between dα/dt and exp (-1/T) thanks to the combination of Eq. (6) and Eq. (7) (kinetic control equation).

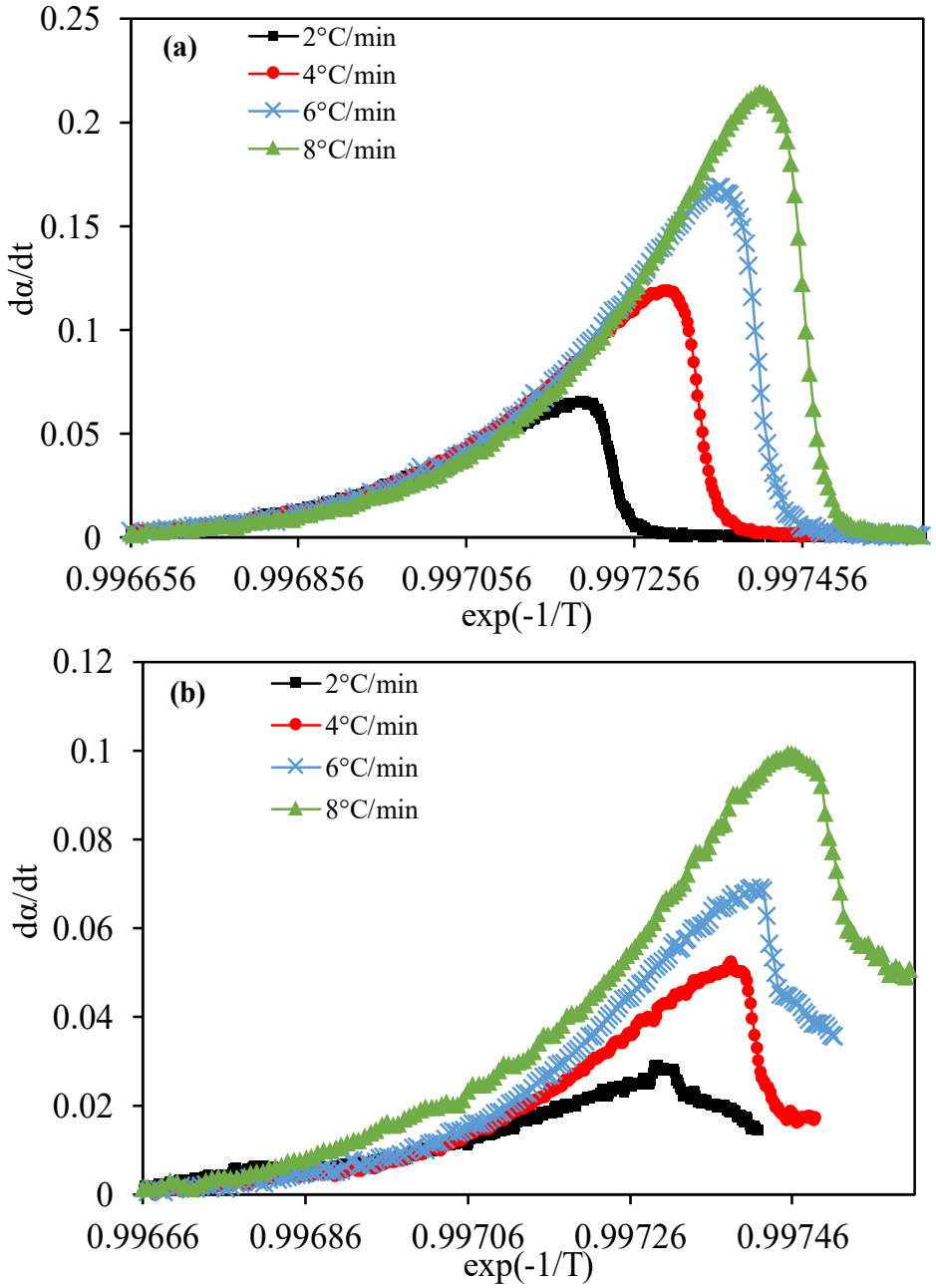


**Fig. 10.** Relationship between dα/dt and exp (-1/T) during the dehydration process of aluminium fumarate (a) and host matrix in AF-$Ca_3$ composite (b).

Aluminium fumarate displayed a single dehydration peak characteristic of host matrix dehydration (Fig. 10a), consistent with the TG-DSC curves discussed earlier. In order to study the impact of host matrix impregnation on the dehydration kinetics, the AF-$Ca_3$ dehydration process was focused on the first peak attributed to support dehydration Fig. 10b. The temperature corresponding to the dehydration peak increases for both solids with an increase in the heating rate, which is in agreement with the previously reported dehydration kinetics of porous materials [37,79].

The apparent activation energy of water desorption ($E_d^{app}$) is then estimated using the methods described by Ozawa [63] (Eq. (8)) and Kissinger [62] (Eq. (9)), which are the most frequently used integral isoconversional methods for experiments performed in non-isothermal conditions, in which the temperature is increased with a constant rate.

$$E_d^{app} = -0.4567 \text{ x R } \frac{d(\log(\beta))}{d(1/T_p)} \quad (8)$$

$$E_d^{app} = \text{R } \frac{dln(\beta/T_p)}{d(1/T_p)} \quad (9)$$

where $\beta$, R, $T_p$ are respectively the heat rate (K $min^{-1}$), the perfect gas constant (J $mol^{-1}$ $K^{-1}$), and the maximum peak temperature (K). The apparent activation energy was calculated from the slope of the curves plotted as $log(\beta_H) = f\left(\frac{10^3}{Tp}\right)$ and $ln\left(\frac{\beta_H}{T_p^2}\right) = f\left(\frac{10^3}{Tp}\right)$ for the Ozawa and Kissinger methods, respectively. The obtained Ozawa and Kissinger curves are reported in Figs. 11a and b, and the activation energy values and the regression coefficients for the two methods are summarized in Table 6.

**Table 6:** Dehydration kinetic data for AF and AF-$Ca_3$ solids.

| Samples | $\beta$ (°C $min^{-1}$) | $T_p$ (°C) | **Kissinger method** | | **Ozawa method** | |
|---|---|---|---|---|---|---|
| | | | Correlation coefficient ($R^2$) | $E_d^{app}$ (kJ $mol^{-1}$) | Correlation coefficient ($R^2$) | $E_d^{app}$ (kJ $mol^{-1}$) |
| **AF** | 2 | 83 | | | | |
| | 4 | 96 | 0.9967 | 48.8 | 0.9973 | 51.6 |
| | 6 | 105 | | | | |
| | 8 | 112 | | | | |
| **AF-$Ca_3$** | 2 | 84 | | | | |
| | 4 | 108 | 0.9908 | 64.6 | 0.9575 | 67.4 |
| | 6 | 113 | | | | |
| | 8 | 120 | | | | |

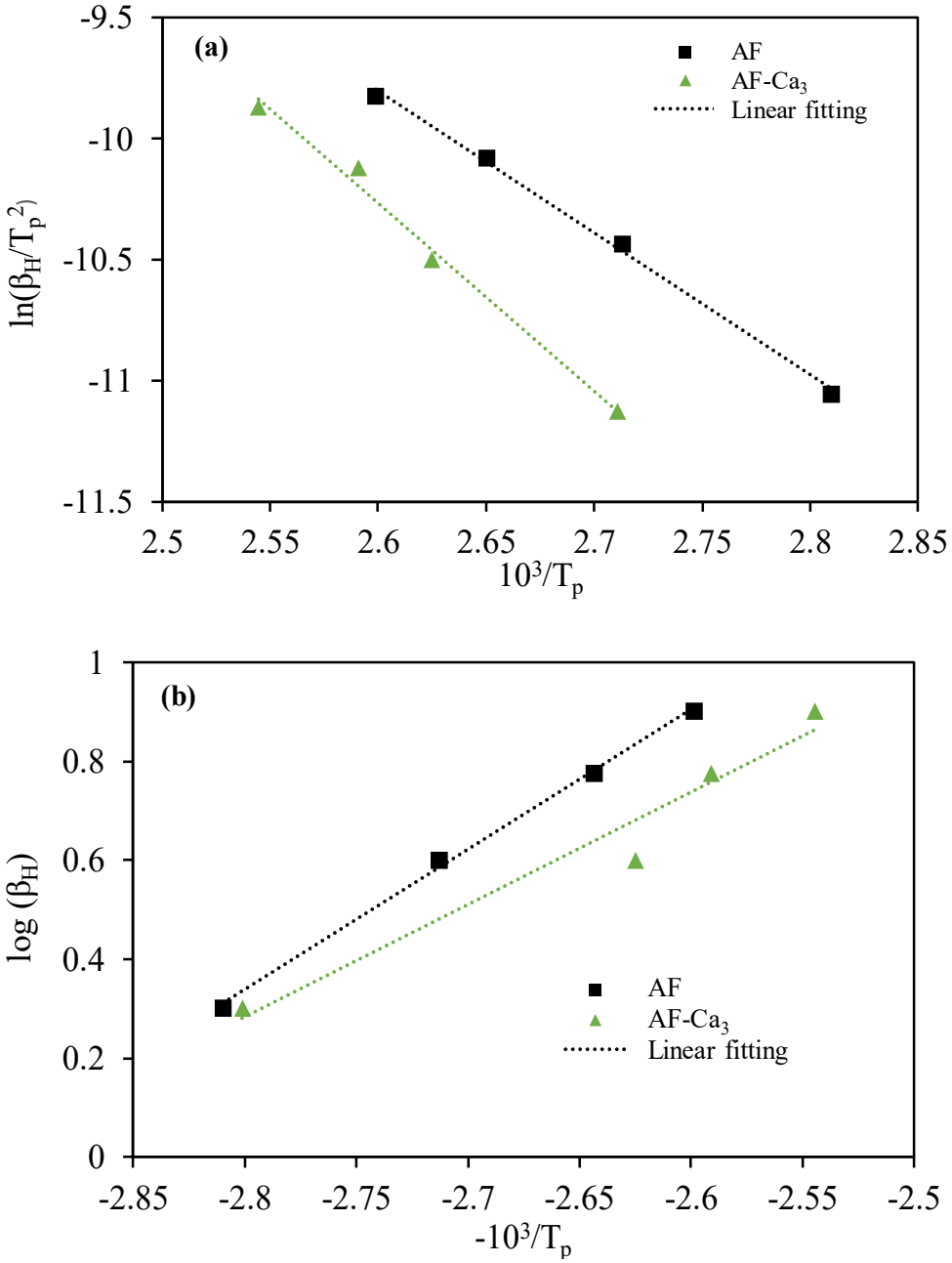


**Fig. 11.** Kissinger (a) and Ozawa (b) linearized equation plots for AF and AF-$Ca_3$ solids.

The good linear fit for both materials and for both methods, and the good agreement between the activation energies calculated by the two methods, indicate the validity and the accuracy of the use of such kinetic methods. Taking into consideration the average of the two dehydration activation energies obtained by the Ozawa and Kissinger methods, the apparent dehydration activation energy of AF is estimated to be 50.2 kJ $mol^{-1}$, lower than the estimated activation energy corresponding to the support dehydration in AF-$Ca_3$ composite (66 kJ mol-

[1]). Thus, addition of $CaCl_2$ into the aluminium fumarate increased the energy required to dehydrate the host matrix in the composite that is in good agreement with the shift of the dehydration peak maxima to higher temperature (Table 6, Fig. 11). This can be explained by the presence of salt on the matrix surface that makes water release more difficult, due to a strong interaction between hygroscopic salt and water, resulting a higher apparent desorption activation energy.

## 4. Conclusion

The storage properties of CSPMs based on the impregnation of aluminium fumarate by $CaCl_2$ have been studied by performing hydration/dehydration cycles in a coupled TG-DSC apparatus. It has been shown that the $CaCl_2$ deposition enhanced the surface affinity for water. The CSPM materials present improved storage performance compared to the host matrix in terms of water sorption/desorption and heat storage/release capacities. Increasing the salt content gradually increases storage performance. Aluminium fumarate impregnated by 58 wt.% of salt (AF-$Ca_3$) present good performances if a limited hydration level is maintained ($CaCl_2.xH_2O$, $x \leq 4$). Despite a decrease of about 5-6 % after 4 dehydration-hydration cycles, the storage performance of AF-$Ca_3$ remains overall stable. Favourable hydration/dehydration kinetics is also fundamental for the applicability of these systems. Water sorption rates of CSPMs are higher than that of pure aluminium fumarate matrix. Although the dehydration activation energy of the support is higher in CSPM materials than in the bare matrix without salt, CSPMs are completely dehydrated at 150 °C, which is suitable for the recovery of a wide range of energy sources [29,61,79]. Their high water and energy storage performances, low desorption temperature as well as good stability over dehydration and hydration cycles make aluminium fumarate-based composites very promising materials for TCHS systems.

## Declaration of competing interest

The authors declare that they have no know competing financial interests or personal relationships that could have appeared to influence the work reported in this paper


## Acknowledgements

This work was supported by the French national Research Agency (Agence Nationale de la Recherche, Projet ANR-18-CE05-0044). The authors are thankful for the scientific services of IRCELYON, particularly P. Mascunan and N. Bonnet for ICP and water sorption isotherms analyses. The authors gratefully acknowledge the Ctμ platform of electronic microscopy (Université de Lyon1).

## References


[1] S. Bellocchi, M. Manno, M. Noussan, M.G. Prina, M. Vellini, Electrification of transport and residential heating sectors in support of renewable penetration: scenarios for the Italian energy system, Energy. 196 (2020) 117062. https://doi.org/10.1016/j.energy.2020.117062.

[2] AIE (2015), Energy Balances of OECD Countries 2015, Editions OCDE, Paris, 2015. [Dataset]

[3] T. Fleiter, R. Elsland, M. Rehfeldt, J. Steinbach, U. Reiter, G. Catenazzi, M. Jakob, C. Dittmann, P. Rivière, Profile of heating and cooling demand in 2015, Heat Roadmap Europe, 2017.

[4] M.Y. Suberu, M.W. Mustafa, N. Bashir, Energy storage systems for renewable energy power sector integration and mitigation of intermittency, Renew. Sustain. Energy Rev. 35 (2014) 499-514. https://doi.org/10.1016/j.rser.2014.04.009.

[5] A.I. Fernandez, M. Martínez, M. Segarra, I. Martorell, L.F. Cabeza, Selection of materials with potential in sensible thermal energy storage, Sol. Energy Mater. Sol. Cells. 94 (2010) 1723–1729. https://doi.org/10.1016/j.solmat.2010.05.035.

[6] B. Zalba, J.M. Marín, L.F. Cabeza, H. Mehling, Review on thermal energy storage with phase change: materials, heat transfer analysis and applications, Appl. Therm. Eng. 23 (2003) 251–283. https://doi.org/10.1016/S1359-4311(02)00192-8.

[7] P. Tatsidjodoung, N. Le Pierrès, L. Luo, A review of potential materials for thermal energy storage in building applications, Renew. Sustain. Energy Rev. 18 (2013) 327–349. https://doi.org/10.1016/j.rser.2012.10.025.

[8] L. Scapino, H.A. Zondag, J. Van Bael, J. Diriken, C.C.M. Rindt, Sorption heat storage for long-term low-temperature applications: a review on the advancements at material and prototype scale, Appl. Energy 190 (2017) 920–948. https://doi.org/10.1016/j.apenergy.2016.12.148.

[9] A.-J. de Jong, F. Trausel, C. Finck, L. van Vliet, R. Cuypers, Thermochemical heat storage – system design issues, Energy Procedia. 48 (2014) 309–319. https://doi.org/10.1016/j.egypro.2014.02.036.

[10] L. André, S. Abanades, G. Flamant, Screening of thermochemical systems based on solid-gas reversible reactions for high temperature solar thermal energy storage, Renew. Sustain. Energy Rev. 64 (2016) 703–715. https://doi.org/10.1016/j.rser.2016.06.043.

[11] A.J. Carrillo, J. González-Aguilar, M. Romero, J.M. Coronado, Solar energy on demand: a review on high temperature thermochemical heat storage systems and materials, Chem. Rev. 119 (2019) 4777–4816. https://doi.org/10.1021/acs.chemrev.8b00315.

[12] K. E. N'Tsoukpoe, F. Kuznik, A reality check on long-term thermochemical heat storage for household applications, Renew. Sustain. Energy Rev. 139 (2021) 110683. https://doi.org/10.1016/j.rser.2020.110683.

[13] D. Aydin, S.P. Casey, S. Riffat, The latest advancements on thermochemical heat storage systems, Renew. Sustain. Energy Rev. 41 (2015) 356–367. https://doi.org/10.1016/j.rser.2014.08.054.

[14] H. Wu, F. Salles, J. Zajac, A critical review of solid materials for low-temperature thermochemical storage of solar energy based on solid-vapour adsorption in view of space heating uses, Molecules 24 (2019) 945. https://doi.org/10.3390/molecules24050945.

[15] J. Cot-Gores, A. Castell, L.F. Cabeza, Thermochemical energy storage and conversion: A-state-of-the-art review of the experimental research under practical conditions, Renew. Sustain. Energy Rev. 16 (2012) 5207–5224. https://doi.org/10.1016/j.rser.2012.04.007.

[16] A.H. Abedin, M.A. Rosen, A critical review of thermochemical energy storage systems, The Open Renew. Energy J. 4 (2011) 42–46. https://doi.org/10.2174/1876387101004010042.

[17] M.M. Farid, A.M. Khudhair, S.A.K. Razack, S. Al-Hallaj, A review on phase change energy storage: materials and applications, Energy Convers. Manag. 45 (2004) 1597-1615. https://doi.org/10.1016/j.enconman.2003.09.015.

[18] P.A.J. Donkers, L. Pel, O.C.G. Adan, Experimental studies for the cyclability of salt hydrates for thermochemical heat storage, J. Energy Storage. 5 (2016) 25-32. https://dx.doi.org/10.1016/j.est.2015.11.005.

[19] J. Jänchen, D. Ackermann, H. Stach, W. Brösicke, Studies of the water adsorption on zeolites and modified mesoporous materials for seasonal storage of solar heat, Solar Energy 76 (2004) 339–344. https://doi.org/10.1016/j.solener.2003.07.036.

[20] J. Jänchen, D. Ackermann, E. Weiler, H. Stach, W. Brösicke, Calorimetric investigation on zeolites, AlPO4's and $CaCl_2$ impregnated attapulgite for thermochemical storage of heat, Thermochim Acta 434 (2005) 37–41. https://doi.org/10.1016/j.tca.2005.01.009.

[21] C. Feng, J. E, W. Han, Y. Deng, B. Zhang, X. Zhao, D. Han, Key technology and application analysis of zeolite adsorption for energy storage and heat-mass transfer process: A review, Renew. Sustain. Energy Rev. 144 (2021) 110954. https://doi.org/10.1016/j.rser.2021.110954.

[22] M.A. Tahat, Heat-pump/energy-store using silica gel and water as a working pair, Appl. Energy 69 (2001) 19-27. https://doi.org/10.1016/S0306-2619(01)00008-3.

[23] E.-P. Ng, S. Mintova, Nanoporous materials with enhanced hydrophilicity and high water sorption capacity, Microporous Mesoporous Mater. 114 (2008) 1–26. https://doi.org/10.1016/j.micromeso.2007.12.022.

[24] A. Gorbach, M. Stegmaier, G. Eigenberger, Measurement and modelling of water vapor adsorption on zeolite 4A-equilibria and kinetics, Adsorption 10 (2004) 29-46. https://doi.org/10.1023/B:ADSO.0000024033.60103.ff.

[25] H. Kakiuchi, S. Shimooka, M. Iwade, K. Oshima, M. Yamazaki, S. Terada, H. Watanabe, T. Takewaki, Water vapor adsorbent FAM-Z02 and its applicability to adsorption heat pump, Kagaku Kogaku Ronbunshu 31 (2005) 273-277. https://doi.org/10.1252/kakoronbunshu.31.273.

[26] G. Basina, D. AlShami, K. Polychronopoulou, V. Tzitzios, V. Balasubramanian, F. Dawaymeh, G.N. Karanikolos, Y. Al Wahedi, Hierarchical AlPO4-5 and SAPO-5 microporous molecular sieves with mesoporous connectivity for water sorption applications, Surface and Coatings Technology. 353 (2018) 378–386. https://doi.org/10.1016/j.surfcoat.2018.08.083.

[27] E. Courbon, P. D'Ans, A. Permyakova, O. Skrylnyk, N. Steunou, M. Degrez, M. Frère, Further improvement of the synthesis of silica gel and $CaCl_2$ composites: enhancement of energy storage density and stability over cycles for solar heat storage coupled with space heating applications, Sol. Energy. 157 (2017) 532–541. https://doi.org/10.1016/j.solener.2017.08.034.

[28] K.C. Chan, C.Y.H. Chao, G.N. Sze-To, K.S. Hui, Performance predictions for a new zeolite 13X/$CaCl_2$ composite adsorbent for adsorption cooling systems, Int. J. Heat Mass Transf. 55 (2012) 3214–3224. https://doi.org/10.1016/j.ijheatmasstransfer.2012.02.054.

[29] S. Hongois, F. Kuznik, P. Stevens, J.-J. Roux, Development and characterisation of a new $MgSO_4$−zeolite composite for long-term thermal energy storage, Sol. Energy Mater. Sol. Cells. 95 (2011) 1831–1837. https://doi.org/10.1016/j.solmat.2011.01.050.

[30] A. Ristić, S.K. Henninger, Sorption composite materials for solar thermal energy s torage, Energy Procedia. 48 (2014) 977–981. https://doi.org/10.1016/j.egypro.2014.02.111.

[31] E.A. Levitskij, Yu.I. Aristov, M.M. Tokarev, V.N. Parmon, "Chemical Heat Accumulators": a new approach to accumulating low potential heat, Sol. Energy Mater. Sol. Cells 44 (1996) 219-235. https://doi.org/10.1016/0927-0248(96)00010-4.

[32] Yu.I. Aristov, G. Restuccia, G. Cacciola, V.N. Parmon, A family of new working materials for solid sorption air conditioning systems, Appl. Therm. Eng. 22 (2002) 191–204. https://doi.org/10.1016/S1359-4311(01)00072-2.

[33] A. Jabbari-Hichri, S. Bennici, A. Auroux, Enhancing the heat storage density of silica–alumina by addition of hygroscopic salts ($CaCl_2$, $Ba(OH)_2$, and $LiNO_3$), Sol. Energy Mater. Sol. Cells. 140 (2015) 351–360. https://doi.org/10.1016/j.solmat.2015.04.032.

[34] Yu. I. Aristov, Nanocomposite sorbents for multiple applications, 1 ed., Jenny Standford Publishing, 2020.

[35] K.E. N'Tsoukpoe, H.U. Rammelberg, A.F. Lele, K. Korhammer, B.A. Watts, T. Schmidt, W.K.L. Ruck, A review on the use of calcium chloride in applied thermal engineering, Appl. Therm. Eng. 75 (2015) 513–531. https://doi.org/10.1016/j.applthermaleng.2014.09.047.

[36] J. Lin, Q. Zhao, H. Huang, H. Mao, Y. Liu, Y. Xiao, Applications of low-temperature thermochemical energy storage systems for salt hydrates based on material classification: A review, Sol. Energy. 214 (2021) 149–178. https://doi.org/10.1016/j.solener.2020.11.055.

[37] A. Jabbari-Hichri, S. Bennici, A. Auroux, $CaCl_2$-containing composites as thermochemical heat storage materials, Sol. Energy Mater. Sol. Cells. 172 (2017) 177–185. https://doi.org/10.1016/j.solmat.2017.07.037.

[38] N. Xie, J. Niu, T. Wu, X. Gao, Y. Fang, Z. Zhang, Fabrication and characterization of $CaCl_2{\cdot}6H_2O$ composite phase change material in the presence of $CsxWO_3$ nanoparticles, Sol. Energy Mater. Sol. Cells. 200 (2019) 110034. https://doi.org/10.1016/j.solmat.2019.110034.

[39] A. Ristić, D. Maučec, S.K. Henninger, V. Kaučič, New two-component water sorbent $CaCl_2$-$FeKIL_2$ for solar thermal energy storage, Microporous Mesoporous Mater.164 (2012) 266–272. https://doi.org/10.1016/j.micromeso.2012.06.054.

[40] H. Furukawa, K.E. Cordova, M. O'Keeffe, O.M. Yaghi, The chemistry and applications of metal-organic frameworks, Science. 341 (2013) 1230444–1230444. https://doi.org/10.1126/science.1230444.

[41] A. Dhakshinamoorthy, A. Santiago-Portillo, A.M. Asiri, H. Garcia, Engineering UiO-66 metal organic framework for heterogeneous catalysis, ChemCatChem. 11 (2019) 899–923. https://doi.org/10.1002/cctc.201801452.

[42] L. Ma, C. Abney, W. Lin, Enantioselective catalysis with homochiral metal–organic frameworks, Chem. Soc. Rev. 38 (2009) 1248. https://doi.org/10.1039/b807083k.

[43] T. Zhang, F. Song, W. Lin, Blocking bimolecular activation pathways leads to different regioselectivity in metal–organic framework catalysis, Chem. Commun. 48 (2012) 8766. https://doi.org/10.1039/c2cc34033j.

[44] O.K. Farha, A.O. Yazaydin, I. Eryazici, C.R. Malliakas, B.G. Hauser, M.G. Kanatzidis, S.T. Nguyen, R.Q. Snurr, J.T. Hupp, De novo synthesis of a metal-organic framework material featuring ultrahigh surface area and gas storage capacities, Nat. Chem 2 (2010) 944-948. https://doi.org/10.1038/nchem.834.

[45] O.V. Gutov, W. Bury, D.A. Gomez-Gualdron, V. Krungleviciute, D. Fairen-Jimenez, J.E. Mondloch, A.A. Sarjeant, S.S. Al-Juaid, R.Q. Snurr, J.T. Hupp, T. Yildirim, O.K. Farha, Water-stable zirconium-based metal-organic framework material with high-surface area and gas-storage capacities, Chem. Eur. J. 20 (2014) 12389–12393. https://doi.org/10.1002/chem.201402895.

[46] X.-G. Wang, Z.-Y. Dong, H. Cheng, S.-S. Wan, W.-H. Chen, M.-Z. Zou, J.-W. Huo, H.-X. Deng, X.-Z. Zhang, A multifunctional metal–organic framework based tumor targeting drug delivery system for cancer therapy, Nanoscale. 7 (2015) 16061–16070. https://doi.org/10.1039/C5NR04045K.

[47] O.K. Farha, I. Eryazici, N.C. Jeong, B.G. Hauser, C.E. Wilmer, A.A. Sarjeant, R.Q. Snurr, S.T. Nguyen, A.Ö. Yazaydın, J.T. Hupp, Metal–organic framework materials with ultrahigh surface areas: is the sky the limit?, J. Am. Chem. Soc. 134 (2012) 15016–15021. https://doi.org/10.1021/ja3055639.

[48] M. Li, D. Li, M. O'Keeffe, O.M. Yaghi, Topological analysis of metal–organic frameworks with polytopic linkers and/or multiple building units and the minimal transitivity principle, Chem. Rev. 114 (2014) 1343–1370. https://doi.org/10.1021/cr400392k.

[49] S.M. Cohen, Postsynthetic methods for the functionalization of metal–organic frameworks, Chem. Rev. 112 (2012) 970–1000. https://doi.org/10.1021/cr200179u.

[50] P. Deria, J.E. Mondloch, O. Karagiaridi, W. Bury, J.T. Hupp, O.K. Farha, Beyond post-synthesis modification: evolution of metal–organic frameworks via building block replacement, Chem. Soc. Rev. 43 (2014) 5896–5912. https://doi.org/10.1039/C4CS00067F.

[51] S.K. Henninger, H.A. Habib, C. Janiak, MOFs as adsorbents for low temperature heating and cooling applications, J. Am. Chem. Soc. 131 (2009) 2776-2777. https://doi.org/10.1021/ja808444z.

[52] P. Küsgens, M. Rose, I. Senkovska, H. Fröde, A. Henschel, S. Siegle, S. Kaskel, Characterization of metal-organic frameworks by water adsorption, Microporous Mesoporous Mater. 120 (2009) 325–330. https://doi.org/10.1016/j.micromeso.2008.11.020.

[53] A. Permyakova, S. Wang, E. Courbon, F. Nouar, N. Heymans, P. D'Ans, N. Barrier, P. Billemont, G. De Weireld, N. Steunou, M. Frère, C. Serre, Design of salt–metal organic framework composites for seasonal heat storage applications, J. Mater. Chem. A. 5 (2017) 12889–12898. https://doi.org/10.1039/C7TA03069J.

[54] W. Shi, Y. Zhu, C. Shen, J. Shi, G. Xu, X. Xiao, R. Cao, Water sorption properties of functionalized MIL-101(Cr)-X (X=-$NH_2$, –$SO_3H$, H, –$CH_3$, –F) based composites as thermochemical heat storage materials, Microporous Mesoporous Mater. 285 (2019) 129–136. https://doi.org/10.1016/j.micromeso.2019.05.003.

[55] N. Tannert, C. Jansen, S. Nießing, C. Janiak, Robust synthesis routes and porosity of the Al-based metal–organic frameworks Al-fumarate, CAU-10-H and MIL-160, Dalton Trans. 48 (2019) 2967–2976. https://doi.org/10.1039/C8DT04688C.

[56] M. Gaab, N. Trukhan, S. Maurer, R. Gummaraju, U. Müller, The progression of Al-based metal-organic frameworks- from academic research to industrial production applications, Microporous Mesoporous Mater. 157 (2021) 131-136. https://doi.org/10.1016/j.micromeso.2011.08.016.

[57] E. Alvarez, N. Guillou, C. Martineau, B. Bueken, B. Van de Voorde, C. Le Guillouzer, P. Fabry, F. Nouar, F. Taulelle, D. de Vos, J.-S. Chang, K.H. Cho, N. Ramsahye, T. Devic, M. Daturi, G. Maurin, C. Serre, The structure of the aluminum fumarate metal-organic framework A520, Angew. Chem. Int. Ed. 54 (2015) 3664–3668. https://doi.org/10.1002/anie.201410459.

[58] H.W.B. Teo, A. Chakraborty, Y. Kitagawa, S. Kayal, Experimental study of isotherms and kinetics for adsorption of water on aluminium fumarate, Int. J. Heat Mass Transf. 114 (2017) 621–627. https://doi.org/10.1016/j.ijheatmasstransfer.2017.06.086.

[59] B. Tan, Y. Luo, X. Liang, S. Wang, X. Gao, Z. Zhang, Y. Fang, In situ synthesis and performance of aluminum fumarate metal–organic framework monolithic adsorbent for water adsorption, Ind. Eng. Chem. Res. 58 (2019) 15712–15720. https://doi.org/10.1021/acs.iecr.9b03172.

[60] E. Elsayed, R. AL-Dadah, S. Mahmoud, A. Elsayed, P.A. Anderson, Aluminium fumarate and CPO-27(Ni) MOFs: characterization and thermodynamic analysis for adsorption heat pump applications, Appl. Therm. Eng. 99 (2016) 802–812. https://doi.org/10.1016/j.applthermaleng.2016.01.129.

[61] J. Ilona, C. William T., D. Amber Waste heat recovery: technology and opportunities in U.S. industry, U.S. department of energy industrial technologies, 2008. https://doi.org/10.2172/1218716.

[62] H.E. Kissinger, Variation of peak temperature with heating rate in differential thermal analysis, J. Res. Natl. Inst. Stand. Technol. 57 (1956) 217. https://doi.org/10.6028/jres.057.026.

[63] T. Ozawa, Kinetic analysis of derivative curves in thermal analysis, J. Therm. Anal. 2 (1970) 301–324. https://doi.org/10.1007/BF01911411.

[64] S. Karmakar, J. Dechnik, C. Janiak, S. De, Aluminium fumarate metal-organic framework: A super adsorbent for fluoride from water, J. Hazard. Mater. 303 (2016) 10–20. https://doi.org/10.1016/j.jhazmat.2015.10.030.

[65] S. Lowell, J.E. Shields, Powder surface area and porosity, Springer Netherlands, Dordrecht, 1991. https://doi.org/10.1007/978-94-015-7955-1.

[66] P. D'ans, E. Courbon, A. Permyakova, F. Nouar, C. Simmonet-Jégat, F. Bourdeux, L. Malet, C. Serre, M. Frère, N. Steunou, A new strontium bromide MOF composite with improved performance for solar energy storage production, J. Energy Storage 25 (2019) 100881. https://doi.org/10.1016/j.est.2019.100881.

[67] I. Alkorta, I. Rozas, J. Elguero, A computational approach to intermolecular proton transfer in the solid state: assistance by proton acceptor molecules, J. Chem. Soc., Perkin Trans. 2 (1998) 2671-2675. 2671–2676. https://doi.org/10.1039/a804677h.

[68] Y. Luo, B. Tan, X. Liang, S. Wang, X. Gao, Z. Zhang, Y. Fang, Investigation on water vapor adsorption performance of LiCl@MIL-100(Fe) composite adsorbent for adsorption heat pumps, Int J Energy Res. (2020) 1-10. https://doi.org/10.1002/er.5361.

[69] I.V. Ponomarenko, I.S. Glaznev, A.V. Gubar, Yu.I. Aristov, S.D. Kirik, Synthesis and water sorption properties of a new composite "$CaCl_2$ confined into SBA-15 pores", Microporous Mesoporous Mater. 129 (2010) 243-250. https://doi.org/10.1016/j.micromeso.2009.09.023.

[70] J. Pátek, J. Klomfar, M. Součková, Solid−liquid equilibrium in the system of $CaCl_2$-$H_2O$ with special regard to the transition points, J. Chem. Eng. Data. 53 (2008) 2260–2271. https://doi.org/10.1021/je800009w.

[71] T. Nonnen, S. Beckert, K. Gleichmann, A. Brandt, B. Unger, H. Kerskes, B. Mette, S. Bonk, T. Badenhop, F. Salg, R. Gläser, A thermochemical long-term heat storage system based on a salt/zeolite composite, Chem. Eng. Technol. 39 (2016) 2427–2434. https://doi.org/10.1002/ceat.201600301.

[72] B Tan, Y. Luo, X. Liang, S. Wang, X. Gao, Z. Zhang, Y. Fang, Composite salt in MIL-101(Cr) with high water uptake and fast adsorption kinetics for adsorption heat pumps, Microporous Mesoporous Mater. 286 (2019) 141-148. https://doi.org/10.1016/J.micromeso.2019.05.039.

[73] J. Canivet, J. Bonnefoy, C. Daniel, A. Legrand, B. Coasne, D. Farrusseng, Structure–property relationships of water adsorption in metal–organic frameworks, New J. Chem. 38 (2014) 3102–3111. https://doi.org/10.1039/C4NJ00076E.

[74] S. Ushak, M. Suárez, S. Véliz, A.G. Fernández, E. Flores, H.R. Galleguillos, Characterization of calcium chloride tetrahydrate as a phase change material and thermodynamic analysis of the results, Renew. Energy 95 (2016) 213–224. https://doi.org/10.1016/j.renene.2016.04.012.

[75] K.K. Meisingset, F. Gronvold, Thermodynamic properties and phase transitions of salt hydrates between 270 and 400 K IV. $CaCI_2.6H_2O$, $CaCl_2.4H_2O$, $CaCl_2.2H_2O$ and $FeCl_3.6H_2O$, J. Chem. Thermodyn. 18 (1986) 159-173. https://doi.org/10.1016/0021-9614(86)90130-8.

[76] Y. Sun, A. Spieß, C. Jansen, A. Nuhnen, S. Gökpinar, R. Wiedey, S.-J. Ernst, C. Janiak, Tunable LiCl@UiO-66 composites for water sorption-based heat transformation applications, J. Mater. Chem. A. 8 (2020) 13364–13375. https://doi.org/10.1039/D0TA03442H.

[77] A. Jabbari-Hichri, A. Auroux, S. Bennici, Effect of NaOH addition on the thermochemical heat storage capacity of nanoporous molecular sieves: Heats of water vapor adsorption on various nanoporous molecular sieves, Int. J. Energy Res. 41 (2017) 1134–1149. https://doi.org/10.1002/er.3697.

[78] S. Vyazovkin, A.K. Burnham, J.M. Criado, L.A. Pérez-Maqueda, C. Popescu, N. Sbirrazzuoli, ICTAC kinetics committee recommendations for performing kinetic computations on thermal analysis data, Thermochim Acta. 520 (2011) 1–19. https://doi.org/10.1016/j.tca.2011.03.034.

[79] P. Gao, X.F. Zhang, L.W. Wang, R.Z. Wang, D.P. Li, Z.W. Liang, A.F. Cai, Study on $MnCl_2/CaCl_2$–$NH_3$ two-stage solid sorption freezing cycle for refrigerated trucks at low engine load in summer, Energy Convers. Manag. 109 (2016) 1-9. https://dx.doi.org/10.1016/j.enconman.2015.11.055.